HHS Public Access

Author manuscript

Dev Cell. Author manuscript; available in PMC 2023 September 26.

Published in final edited form as:

Dev Cell. 2022 September 26; 57(18): 2204–2220.e6. doi:10.1016/j.devcel.2022.08.011.

RIPOR2-mediated autophagy dysfunction is critical for aminoglycoside-induced hearing loss

Jinan Li[1], **Chang Liu**[1], **Ulrich Müller**[2], **Bo Zhao**[1,3,*]

[1]Department of Otolaryngology-Head and Neck Surgery, Indiana University School of Medicine, Indianapolis, IN 46202, USA.

[2]The Solomon H. Snyder Department of Neuroscience, Johns Hopkins University School of Medicine, Baltimore, MD 21205, USA.

[3]Lead contact

SUMMARY:

Aminoglycosides (AGs) are potent antibiotics capable of treating a wide variety of life-threatening infections, however, they are ototoxic and cause irreversible damage to cochlear hair cells. Despite substantial progress, little is known about the molecular pathways critical for hair cell function and survival that are affected by AG exposure. We demonstrate here that gentamicin, a representative AG antibiotic, binds to and triggers within minutes translocation of RIPOR2 in murine hair cells from stereocilia to the pericuticular area. Then, by interacting with a central autophagy component GABARAP, RIPOR2 affects autophagy activation. Reducing the expression of RIPOR2 or GABARAP completely prevents AG-induced hair cell death and subsequent hearing loss in mice. Additionally, abolishing the expression of PINK1 or Parkin, two key mitochondrial autophagy proteins, prevents hair cell death and subsequent hearing loss caused by AG. In summary, our study demonstrates that RIPOR2-mediated autophagic dysfunction is essential for AG-induced hearing loss.

In brief

Li et al. find that aminoglycoside binds to and triggers rapid translocation of RIPOR2 in cochlear hair cells. RIPOR2 interacts with the core autophagy component GABARAP and affects autophagy activation. Inhibiting this pathway prevents aminoglycoside-induced hearing loss, suggesting that autophagy pathway components are potential therapeutic targets for preventing aminoglycoside ototoxicity.

Graphical Abstract

*Correspondence: zhaozb@iu.edu.

AUTHOR CONTRIBUTIONS: J.L. performed the experiments. C.L. purified proteins. B. Z. and U.M. planned the study and wrote the manuscript.

COMPETING INTERESTS: Dr. Müller is a co-founder of Decibel Therapeutics. J.L., U.M. and B. Z. are named inventors on patent applications related to this work.

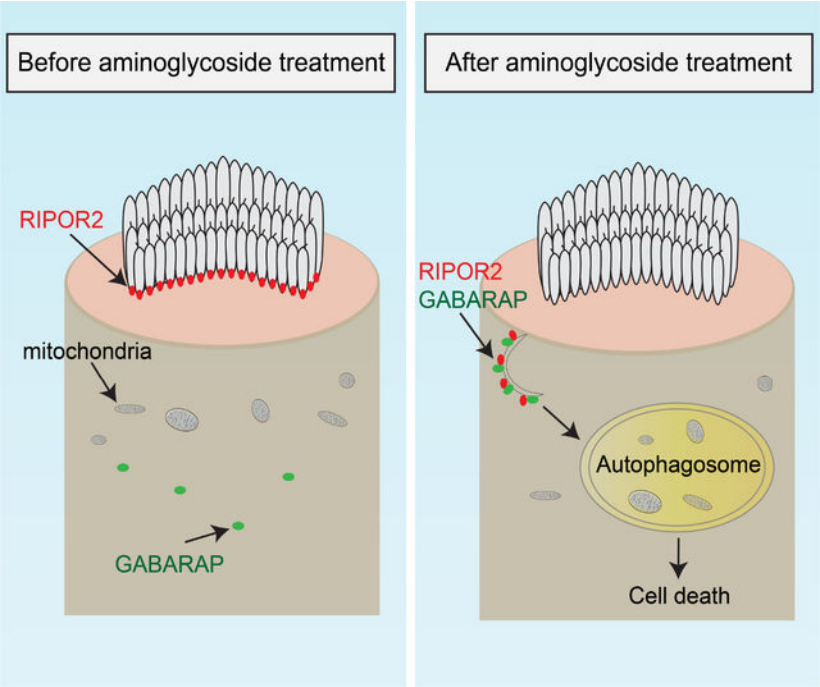

RIPOR2, Rho family-interacting cell polarization regulator 2;
GABARAP, Gamma-aminobutyric acid receptor-associated protein

Keywords

RIPOR2; GABARAP; autophagy; mitophagy; aminoglycoside; hearing loss; ototoxicity; hair cell

INTRODUCTION:

Aminoglycosides (AGs) are widely used to treat serious infections, as they are highly potent against many multidrug-resistant Gram-negative organisms. Unfortunately, systemically administered AGs exhibit strong ototoxicity and lead to irreversible cochlear damage, in both humans and experimental animals. By audiometry, hearing loss is found in about 20–47% of patients that received AG therapy (Fausti et al., 1992; Huth et al., 2015; Huth et al., 2011). However, due to their affordable cost and low incidence of antibiotic resistance, AGs are often selected as a first line of treatment especially in the developing world (O'Sullivan et al., 2017).

Over the years, significant insights have been obtained into the mechanisms by which AGs disrupt cochlear function. Systemically administered AGs are trafficked across the blood-endolymph barrier and preferentially enter hair cells, the specialized mechanosensory cells of the inner ear that convert sound-induced vibrations into electrochemical signals (Li and Steyger, 2011). The major entry route for AGs into hair cells are the mechanotransduction (MET) channels that are localized near the tips of stereocilia that crown the apical surface of hair cells (Alharazneh et al., 2011; Beurg et al., 2009; Marcotti et al., 2005; Vu et al., 2013) (Figure 1A). After entering hair cells, AGs initiate a series of cellular responses that eventually result in hair cell death (Huth et al., 2011). Humans with mitochondrial DNA

mutations in the 12S rRNA gene are more susceptible to AG ototoxicity, implying that mitochondria play an essential role in AG ototoxicity (Guan, 2011; Prezant et al., 1993). In addition, reactive oxygen species (ROS) are thought to contribute to hair cell death following AG exposure (Clerici et al., 1995; Hirose et al., 1997), and deregulation of autophagy may also be involved (He et al., 2017; Kim et al., 2017).

Autophagy is thought to safeguard cells by removing undesired molecules and damaged subcellular organelles, but aberrant or inappropriately triggered autophagy can cause cell damage and death (Xie and Zhou, 2018). Notably, peroxisomal autophagy plays a critical role in noise-induced hearing loss (Delmaghani et al., 2015), and AG exposure induces autophagy in hair cells (He et al., 2017; Kim et al., 2017). However, the extent to which autophagy contributes to AG ototoxicity is controversial (Draf et al., 2021; He et al., 2017; Kim et al., 2017). Most studies are based on the analysis of the effects of pharmacological inhibitors/activators (Draf et al., 2021; He et al., 2017; Kim et al., 2017), which may affect other cellular pathways and/or cause dose-dependent hair cell damage (Draf et al., 2021; Leitmeyer et al., 2015; Li et al., 2014). Thus, further studies are necessary to define the mechanisms by which AG treatment affects hair cell survival.

In the current study, we have identified components of the molecular pathway that is essential to trigger the cytotoxic effects of AGs in hair cells. Surprisingly, we found that AGs bind to RIPOR2/Fam65b, which forms a circumferential ring structure at the stereocilia base, and is required for stereocilia morphogenesis (Diaz-Horta et al., 2018; Zhao et al., 2016) (Figure 1A). Importantly, AGs have to traverse this narrow part of stereocilia after entering through MET channel before reaching the cell body. Unexpectedly, AGs trigger rapid subcellular translocation of RIPOR2 from the base of stereocilia to the region of the pericuticular necklace in hair cells. RIPOR2 then interacts with GABARAP, a component of the autophagy pathway that has major roles in the removal and recycling of dysfunctional cellular components to maintain cellular homeostasis and health (Klionsky et al., 2021). Strikingly, reducing RIPOR2 or GABARAP expression completely prevents hair cell death and subsequent hearing loss caused by AG when systemically administered. Additionally, we found that disrupting the mitochondrial autophagy pathway by abolishing the expression of PINK1 or Parkin protects hair cells from AG ototoxicity. Taken together, our findings delineate molecular components of a pathophysiological response pathway induced by AGs in hair cells that ultimately affect the autophagy pathway thus causing hair cell dysfunction and death. Our findings also identify that the autophagy pathway is a highly promising therapeutic target for preventing hearing loss caused by AGs, and possibly by other insults that affect the inner ear.

RESULTS:

Rapid translocation of RIPOR2 triggered by GEN

To identify AG binding proteins in hair cells, gentamicin (GEN) pull-down assays were performed using lysates from HEI-OC1 cells, a mouse inner ear cell line (Kalinec et al., 2016) (Figure S1A). Using Nanoflow Liquid Chromatography with tandem mass spectrometry (LC-MS/MS), a total of about 300 proteins were subsequently identified. Myh9, a RIPOR2 binding protein (Diaz-Horta *et al.*, 2018), was detected in high quantities.

RhoC, another RIPOR2 binding protein (Zhao *et al.*, 2016), was also detected (Supplemental Table 1). To supplement LC-MS/MS, which could miss certain proteins such as those that were not adequately digested to peptides, we performed immunoblot analysis to determine if RIPOR2 is a GEN binding protein. Immunoblot analysis indicates that GEN interacts with RIPOR2 (Figure 1B). To confirm this finding, we expressed GFP-tagged RIPOR2 in HEK293 cells. GFP-RIPOR2 was captured using GEN-conjugated beads (Figure 1C). In the presence of competitive soluble GEN, interaction of GEN-conjugated beads with RIPOR2 was reduced (Figure 1C). Additionally, GEN pull-down assay using purified RIPOR2 protein demonstrated that GEN binds to RIPOR2 directly (Figures 1D and S1B). No interaction was detected between GEN and GRXCR2, taperin or CLIC5, which colocalize with RIPOR2 at the stereocilia base and are associated with human hearing loss (Gagnon et al., 2006; Imtiaz et al., 2014; Li et al., 2010; Liu et al., 2018; Rehman et al., 2010; Seco et al., 2015) (Figures S1C–S1E). These results suggest that RIPOR2 is a GEN-binding protein.

Next, immunostaining was performed to investigate whether GEN affects RIPOR2 expression or localization in cochlear hair cells. Cochlear explants dissected from postnatal day 4 (P4) wild-type mice were treated with 1 mM GEN for 2.5, 5, 15, 30, 60, or 120 minutes. RIPOR2 localized at the stereocilia base in untreated hair cells (Figure 1E). Remarkably, 2.5 minutes after GEN exposure, RIPOR2 had translocated to the pericuticular area (Figure 1E). Within 15 minutes of treatment, more than 80% of the RIPOR2 signal was detected in the pericuticular area in inner hair cells (IHCs) (Figures 1E, 1F, S1F–S1H, and Supplemental Videos 1 and 2). RIPOR2 accumulation at the stereocilia base was restored within 2 hours after continued exposure to 1 mM GEN (Figures 1E and 1F). RIPOR2 translocated rapidly to the pericuticular area in IHCs located in the cochlea's apical, middle and basal regions (Figures S1I–S1K). Basal IHCs had more translocated RIPOR2 than apical hair cells (Figure S1L), consistent with previous findings that basal hair cells accumulate more AG (Alharazneh et al., 2011). Additionally, at all developmental stages studied, GEN induced rapid RIPOR2 translocation (Figure S1M). To investigate whether GEN at lower concentrations could induce RIPOR2 translocation, hair cells were treated with GEN at various concentrations for 15 minutes. RIPOR2 translocation was observed in a large number of IHCs treated with 0.1 mM GEN, whereas 0.25 mM or 0.5 mM GEN induced rapid RIPOR2 translocation in nearly all IHCs (Figure 1G). Redistribution of RIPOR2 was also observed in outer hair cells (OHCs) following GEN exposure (Figures 1H, S1N).

Rapid translocation of RIPOR2 triggered by different types of AGs

AGs are classified into several groups based on their structure and might cause ototoxicity via different mechanisms (Krause et al., 2016). To investigate the effect of various AGs on the cellular distribution of RIPOR2, cochlear explants were treated with kanamycin (KAN), amikacin, neomycin, streptomycin or apramycin. All tested AGs, but none of the other types of antibiotics examined, induced rapid RIPOR2 translocation (Figures S2A–S2E), suggesting that AGs activate a common molecular pathway in hair cells. Apramycin induced weaker relocalization of RIPOR2 than other tested AGs (Figures S2C and S2D), which correlates with its lower ototoxicity (Matt et al., 2012). Cisplatin is a widely used chemotherapeutic agent with strong ototoxicity. Hair cells take up cisplatin,

like AGs, requiring functional MET (Li et al., 2022; Thomas et al., 2013). Cisplatin treatment had no effect on the RIPOR2 distribution in hair cells (Figure S2F). Next, we immunolocalized taperin, GRXCR2 and CLIC5in hair cells following GEN exposure. There was no discernible change in the distribution of these proteins (Figures S2G–S2I). These findings suggest that relocalization of RIPOR2 is specifically triggered by AGs.

RIPOR2 translocation triggered by AGs requires AGs to enter hair cells via MET channels

The MET channel is the major entry route for AGs in hair cells (Alharazneh et al., 2011; Marcotti et al., 2005; Vu et al., 2013). TMIE is an obligatory subunit of the MET channel and channel function is abolished in hair cells lacking TMIE (Cunningham et al., 2020; Zhao et al., 2014). Cochlear explants were dissected from *Tmie*$^{-/-}$ mice and incubated with GEN-conjugated Texas Red (GTTR) for 15 min. As expected, there was no GTTR uptake in *Tmie*$^{-/-}$ hair cells (Figures 2A and 2B). *Ripor2*$^{+/-}$ hair cells took up GTTR in the same manner as wild-type hair cells, suggesting that reducing RIPOR2 expression does not affect GEN uptake (Figures 2C and 2D). To confirm this finding, wild-type and *Ripor2*$^{+/-}$ cochlear explants were fixed following GEN treatment, and stained with an antibody against GEN. There was no difference in GEN uptake between wild-type and *Ripor2*$^{+/-}$ hair cells (Figure S3A).

To investigate whether GEN-induced RIPOR2 translocation requires functional MET channels, *Tmie*$^{-/-}$ cochlear explants were treated with 1 mM GEN for 15 minutes. In *Tmie*$^{-/-}$ mice, GEN treatment did not induce RIPOR2 relocalization to the pericuticular necklace (Figures 2E and 2F). Additionally, when MET was blocked by the addition of EGTA or benzamil (Rusch et al., 1994), GEN did not induce RIPOR2 relocalization (Figures 2G, 2H, S3B and S3C). These findings suggest that the translocation of RIPOR2 induced by AGs requires the entrance of AGs into hair cells via MET channels.

Effects of translation and reactive oxygen species

Previous studies suggest that AGs affect protein translation (Francis et al., 2013; Huth et al., 2011). GEN does not affect *Ripor2* mRNA level in murine hair cells (Tao and Segil, 2015). To investigate further a potential role of defects in protein synthesis in GEN-induced RIPOR2 translocation, cochlear explants were pretreated with cycloheximide (CHX), a protein synthesis inhibitor (Matsui et al., 2002; Zhao et al., 1996). CHX had no effect on RIPOR2 redistribution following GEN treatment (Figures S3D–S3G), suggesting that AGs' effects on RIPOR2 are not due to changes in protein synthesis but rather to changes in the cellular distribution of already available RIPOR2 protein.

Previous studies have shown that AGs increase the accumulation of ROS in hair cells, implying a critical role of the ROS cascade in AG-induced ototoxicity (Clerici et al., 1995; Hirose et al., 1997). To investigate whether abnormally accumulated ROS trigger RIPOR2 translocation, cochlear explants were treated with 1 mM hydrogen peroxide (H_2O_2) for 15 minutes. H_2O_2 treatment did not affect RIPOR2 localization (Figures S3H, S3I). The next question was whether we could prevent RIPOR2 translocation by lowering ROS levels. Thus, hair cells were pretreated overnight with 1 mM antioxidant reduced glutathione (GSH) or D-Methionine (D-Met). These pretreatments had no effect on GEN-induced RIPOR2

translocation (Figures S3J–S3L). These findings suggest that accumulated ROS do not initiate RIPOR2 translocation but may perhaps act downstream of it.

Reducing RIPOR2 expression prevents AG-induced hair cell death and subsequent hearing loss

To investigate the extent to which RIPOR2 contributes to AG ototoxicity, we subcutaneously injected AGs into wild-type control mice and heterozygous *Ripor2*$^{+/-}$ mice. Critically, RIPOR2 protein levels are substantially reduced in *Ripor2*$^{+/-}$ mice (Figures S4A–S4C). Due to the fact that GEN is highly toxic to mice leading to high mortality upon systemic administration of GEN, mice were injected with KAN, which also induces RIPOR2 translocation (Figures S2A). Cochleae were dissected and scanning electron microscopy was performed after subcutaneous injection with 800 mg/kg KAN twice daily for 14 consecutive days. Only ~24% of hair cells, mainly IHCs, survived in wild-type mice following KAN treatment (Figures 3A and 3C). *Ripor2*$^{+/-}$ hair cells had hair bundles with the typical V-shape, normal MET and GTTR uptake (Zhao et al., 2016; Figures 2C and 3A). Surprisingly, no significant hair cell loss was observed in *Ripor2*$^{+/-}$ mice following KAN treatment (Figures 3A and 3C). To confirm this finding, mice were injected with 1200 mg/kg KAN, a dose close to the median lethal dose (LD50) of KAN (Lewis, 2004). No significant hair cell loss was observed in *Ripor2*$^{+/-}$ mice (Figures 3A and 3C). These results suggest that reducing RIPOR2 expression protects hair cells from AG-induced death.

GRXCR2, like RIPOR2, is required for stereocilia morphogenesis and auditory perception (Avenarius et al., 2018; Liu et al., 2018). No translocation of GRXCR2 was observed in hair cells following AG treatment (Figure S2G). Different to *Ripor2*$^{+/-}$ mice, *Grxcr2*$^{+/-}$ mice lost over 75% of hair cells, following KAN treatment (Figures 3B and 3C). As a further control, we analyzed *Tmie*$^{+/-}$ mice. Significant hair cell loss was observed in *Tmie*$^{+/-}$ mice following KAN treatment (Figures S4D and S4E), suggesting that reducing *Tmie* expression only partially protects against KAN-induced hair cell death, most likely by affecting AG uptake (Figure 2A).

Next, auditory brainstem responses (ABRs) to broadband click stimuli were measured in wild-type and *Ripor2*$^{+/-}$ mice, to determine whether reducing RIPOR2 expression could prevent AG-induced hearing loss. The hearing thresholds of control *Ripor2*$^{+/-}$ mice were similar to those of wild-type mice, indicating that depleting one copy of *Ripor2* in the genome had no effect on normal hearing (Figure 3D). After 14 days of KAN treatment, wild-type mice were profoundly deaf (Figure 3D). Remarkably, KAN administration did not significantly elevate the hearing thresholds of *Ripor2*$^{+/-}$ mice (Figure 3D), consistent with the minimal hair cell loss observed in *Ripor2*$^{+/-}$ mice (Figure 3A). Additionally, recording ABRs in response to pure tones demonstrated that KAN significantly elevated hearing thresholds across the entire analyzed frequency spectrum in wild-type mice, but not in *Ripor2*$^{+/-}$ mice (Figure 3E).

Next, we injected 1400 mg/kg KAN to *Ripor2*$^{+/-}$ mice for 14 days, above the LD50 of KAN. No significant hearing-threshold elevation was observed (Figures S4F and S4G). To investigate whether KAN has any long-term toxicity, *Ripor2*$^{+/-}$ mice were treated with 1200 mg/kg KAN for 14 days and ABRs were measured after 2 and 4 weeks. No

significant hearing-threshold elevation was observed (Figures S4H and S4I). Following KAN treatment, *Grxcr2*$^{+/-}$ and *Tmie*$^{+/-}$ mice had profound hearing loss or significantly elevated hearing thresholds respectively, consistent with the robust hair cell death induced by KAN (Figures S4J–S4M). Thus, our data unequivocally demonstrate that RIPOR2 is critical for AG-induced hearing loss.

GABARAP interacts with RIPOR2 and is not required for normal hearing

To gain mechanistic insights into the pathophysiological response of hair cells to AGs that depend on RIPOR2, we used full-length RIPOR2 as the bait to screen a previously constructed inner ear specific yeast two-hybrid library (Zhao et al., 2014; Zhao et al., 2016). We found that GABARAP and GABARAPL1, which are yeast Atg8 orthologues and key autophagy proteins (Nguyen et al., 2016; Vaites et al., 2018), interact with RIPOR2 (Figure S5A). Co-immunoprecipitation (Co-IP) experiments were performed to confirm the yeast two-hybrid results. RIPOR2-GFP co-immunoprecipitated with HA-tagged GABARAP and GABARAPL1, but not with LC3β, another mammalian yeast Atg8 orthologue (Figure 4A). To investigate the functions of GABARAP, we phenotyped a *Gabarap*-mutant mouse, in which a *LacZ* expression cassette was inserted in the *Gabarap* genomic locus. As shown by X-gal staining, *Gabarap* was abundantly expressed in IHCs and OHCs (Figure 4B), consistent with previous RNA-seq data (Scheffer et al., 2015). Cochlear tissue was dissected from homozygous P7 *Gabarap* mutants and western blotting was performed. A GABARAP-specific antibody detected a ~14 kDa protein in wild-type mice but not in mutants, suggesting that the mouse is a null mutant, which will be referred to as *Gabarap*$^{-/-}$ mice hereafter (Figure 4C).

Next, we immunolocalized GABARAP in hair cells. GABARAP was distributed in a punctate pattern throughout the cell body of wild-type hair cells but not in their stereocilia. No signal was detected in *Gabarap*$^{-/-}$ hair cells (Figure 4D), confirming the specificity of the antibody. Notably, we did not observe any significant change of GABARAP in *Ripor2* mutant hair cells (Figures 4C and 4D), suggesting that reducing or abolishing RIPOR2 expression does not affect GABARAP expression or localization. As shown by immunostaining and scanning electron microscopy, stereocilia morphology and RIPOR2 localization were unaffected in *Gabarap*$^{-/-}$ hair cells (Figures 4E, 4F and 6A). Additionally, *Gabarap*$^{-/-}$ mice had normal GEN uptake and hearing (Figures S5B, S5C, 4G and 4H).

RIPOR2 colocalizes with and activates GABARAP in the pericuticular area following AG exposure

We immunolocalized GABARAP in P4 wild-type hair cells following GEN treatment. Without AG treatment, limited GABARAP signal was observed in the stereociliary or pericuticular regions (Figure 5A). Notably, 5 minutes and 15 minutes following GEN treatment, GABARAP accumulated in the pericuticular area, where it colocalized with translocated RIPOR2. RIPOR2 translocated back to the stereocilia base 2 hours after continued exposure to GEN, whereas GABARAP was retained in the pericuticular area (Figure 5A). GABARAP has been shown to regulate the cell surface expression of a variety of receptors and ion channels in some cellular contexts (Schaaf et al., 2016). To investigate whether GABARAP could regulate GEN-induced RIPOR2 translocation, P4 *Gabarap*$^{-/-}$ hair

cells were treated with GEN. RIPOR2 translocation was minimally affected, suggesting that GABARAP is not required for RIPOR2 translocation (Figures 5B and 5C). Remarkably, no significant accumulation of GABARAP was observed in the pericuticular area of *Ripor2*$^{+/-}$ hair cells, suggesting that RIPOR2 either recruits GABARAP to the pericuticular area or stabilizes GABARAP in that region, following GEN treatment (Figure 5D).

Next, we sought to determine whether RIPOR2 is required for GABARAP lipidation, which is necessary for the autophagic function of GABARAP (Klionsky et al., 2021; Klionsky et al., 2016). Following GEN treatment, there was a significant increase in lipidated GABARAP-II in P4 wild-type cochlear explants, but not in *Ripor2*$^{+/-}$ samples (Figures 5E–5G). These findings suggest that RIPOR2 acts upstream of GABARAP during GEN treatment by regulating GABARAP translocation and activation. Consistent with previous studies (He et al., 2017; Kim et al., 2017), there was a significant increase in lipidated LC3β in wild-type cochlear explants following GEN treatment, suggesting the activation of autophagy (Figures 5H and 5J). No significant elevation of lipidated LC3β was observed in *Ripor2*$^{+/-}$ or *Gabarap*$^{-/-}$ samples (Figures 5I and 5J), suggesting that RIPOR2 and GABARAP are required for LC3β activation following AG treatment. Then, cochlear explants were labeled with DAPGreen, which is used to detect autophagy in living cells (Iwashita et al., 2018). Two hours after GEN treatment, wild-type hair cells exhibited a ~2.5-fold increase in DAPGreen signals, but *Ripor2*$^{+/-}$ and *Gabarap*$^{-/-}$ hair cells had just a minor increase (Figures 5K–5M), suggesting that RIPOR2 and GABARAP are essential for GEN-induced autophagy activation.

GABARAP is essential for AG-induced hair cell death and subsequent hearing loss

To determine whether GABARAP is required for AG ototoxicity, 1200 mg/kg KAN was subcutaneously injected into wild-type, *Gabarap*$^{+/-}$ and *Gabarap*$^{-/-}$ mice for 14 days. Robust hair cell death was observed in KAN-treated wild-type mice. Similar to *Ripor2*$^{+/-}$ mice, neither *Gabarap*$^{+/-}$ nor *Gabarap*$^{-/-}$ mice showed significant hair cell loss following KAN treatment (Figures 6A and 6B). Consistently, KAN treatment had no effect on hearing thresholds in *Gabarap*$^{+/-}$ or *Gabarap*$^{-/-}$ mice (Figures 6C and 6D). These results suggest that GABARAP is essential for AG ototoxicity.

Then, we sought to determine the functions of autophagy pathway in AG ototoxicity. RIPOR2 and GABARAP are critical for LC3β lipidation following AG treatment. To determine the extent to which LC3β is involved in AG ototoxicity, *LC3β*$^{-/-}$ mice (Cann et al., 2008) were characterized, which have normal stereociliary morphology, RIPOR2 and GABARAP localization, GEN uptake, and hearing (Figures S6, 6F and 6G). Similar to *Ripor2*$^{+/-}$, *Gabarap*$^{+/-}$ and *Gabarap*$^{-/-}$ mice, there was no significant loss of hair cells or elevation in hearing thresholds in *LC3β*$^{-/-}$ mice following 1200 mg/kg KAN treatment (Figures 6E–6G, S6I). These findings strongly suggest that the autophagy pathway is critical for AG ototoxicity.

PINK1 and Parkin are required for AG-induced hair cell death and subsequent hearing loss

In humans, mutations in the mitochondrial 12S rRNA are associated with an increased susceptibility to AG ototoxicity, implying that mitochondria play a significant role (Guan,

2011; Prezant et al., 1993). Notably, cells with mutations in the mitochondrial 12S rRNA exhibit elevated mitophagy, which is mitochondrial-specific autophagy (Yu et al., 2014). To determine whether mitophagy is activated in hair cells following AG treatment, cochlear explants were labeled with Mtphagy dye, a dye used to detect mitophagy in live cells. Following GEN treatment, Mtphagy signals were significantly increased in wild-type hair cells, but not in *Ripor2*$^{+/-}$ or *Gabarap*$^{-/-}$ hair cells (Figures 7A–7C and S7A), suggesting that RIPOR2 and GABARAP are critical for the activation of mitophagy following GEN treatment. Previous studies reported a decrease in mitochondrial membrane potential (MtMP) in hair cells treated with AG (Dehne et al., 2002; Owens et al., 2007), which may indicate impaired mitochondrial function and lead to mitophagy (Elmore et al., 2001). Consistent with these findings, the MtMP deceased in wild-type hair cells following GEN treatment, but not in *Ripor2*$^{+/-}$ or *Gabarap*$^{-/-}$ hair cells (Figures 7D and S7B).

To further elucidate the extent to which mitophagy is required for AG-induced ototoxicity, we investigated the functions of PINK1 or Parkin, two key mitophagy proteins (Eiyama and Okamoto, 2015), by characterizing corresponding knockout mice (referred as *Pink1*$^{-/-}$ and *Prkn*$^{-/-}$ mice, respectively) (Goldberg et al., 2003; Kitada et al., 2007). Stereocilia morphology, GEN uptake, and RIPOR2 and GABARAP localization were unaffected in *Pink1*$^{-/-}$ and *Prkn*$^{-/-}$ hair cells (Figures S7C–S7K).

Next, we investigated whether PINK1 or Parkin is required for AG ototoxicity. Heterozygous and homozygous *Pink1* and *Prkn* mutant mice received KAN for 14 days. Remarkably, KAN treatment did not result in significant hair cell loss in *Pink1*$^{+/-}$, *Pink1*$^{-/-}$ or *Prkn*$^{-/-}$ mice (Figure 7E). Approximately 20% of hair cells died in heterozygous *Prkn*$^{+/-}$ mice after KAN treatment, suggesting that depleting one allele of *Prkn* protects, but not fully, against AG-induced hair cell death (Figures 7E). These findings suggest that reducing or eliminating *Pink1* or *Prkn* expression prevents AG-induced hair cell death.

ABRs in *Pink1* mutant mice were then analyzed. Both *Pink1*$^{+/-}$ and *Pink1*$^{-/-}$ mice had normal hearing at 5 weeks of age. No significant increases in hearing thresholds were observed in *Pink1*$^{+/-}$ or *Pink1*$^{-/-}$ mutant mice following KAN treatment (Figures 7F and 7G). Next, we sought to determine whether *Prkn* is required for AG-induced hearing loss. Consistent with 20% hair cell death in heterozygous *Prkn*$^{+/-}$ mice following KAN administration, moderate hearing loss was observed in the treated mice (Figures 7F and 7H). Although control homozygous *Prkn*$^{-/-}$ mice had a ~15 dB higher hearing threshold than wild-type mice at high-frequencies prior to KAN treatment, KAN treatment did not result in a significant increase in hearing thresholds in *Prkn*$^{-/-}$ mice (Figures 7F and 7H). These results suggest that PINK1 and Parkin are critical for AG ototoxicity.

DISCUSSION:

Systemically administered AGs damage the cochlear organ by disrupting hair cell function thus leading to permanent hearing loss. This pathophysiological response is a significant drawback for the use of AGs to treat life-threating infections caused by Gram-negative bacteria. It would be desirable to define the mechanisms by which AGs affect hair cell function, in order to devise strategies that maintain their antimicrobial activity but do not

negatively affect the auditory sensory organ. Here we identified a molecular pathway in hair cells that is critical for the pathophysiological response of hair cells to AG treatment. Surprisingly, we show that RIPOR2, which is linked to genetic forms of hearing loss in humans (de Bruijn et al., 2020; Diaz-Horta et al., 2014), is essential for AG-induced hair cell death. This was unexpected since our previous studies have shown that RIPOR2 is localized to the base of hair cell stereocilia where it has a morphogenetic role in shaping and maintaining the stereocilia of hair cells (Zhao et al., 2016). Our findings suggest that RIPOR2 interacts with components of the autophagy pathway and that a specific form of autophagy, mitophagy, is affected by AG treatment in a RIPOR2-dependent manner. Importantly, AG-induced hair cell death and hearing loss are not observed in several mouse models with mutations in components of the autophagy pathway, highlighting the importance of this pathway for the pathophysiological response to AGs (Figure 7I).

Our data show that RIPOR2 binds to AG antibiotics and rapidly translocates upon AG-treatment from the base of stereocilia to the pericuticular necklace. How AGs lead to this translocation is currently unclear, but the fact that RIPOR2 binds to AGs suggests that AG might competitively inhibit interactions of RIPOR2 with binding partners at the base of stereocilia such as RhoC (Zhao et al., 2016). Several myosins, such as Myo7A, Myo6, Myo1C and Myh9, localize in the cuticular area and/or stereocilia and interact with RIPOR2 (Cyr et al., 2002; Diaz-Horta et al., 2018; Hasson et al., 1997). One intriguing possibility is that certain myosin(s) may be involved in AG ototoxicity through regulating RIPOR2 translocation. A similar translocation from the cell body to the pericuticular necklace is observed for GABARAP, which we have identified as a binding partner for RIPOR2. Since translocation of GABARAP depends on RIPOR2, the findings suggest that RIPOR2 recruits or stabilizes GABARAP in the pericuticular necklace in response to AG treatment. However, while RIPOR2 is only transiently localized to the pericuticular necklace following AG treatment, GABARAP localization to this subcellular structure is maintained for hours, suggesting that other mechanisms must be involved in its retention. Furthermore, we observed RIPOR2 translocation back to the base of stereocilia, indicating that another molecular pathway may regulate RIPOR2 translocation back to the base of stereocilia to maintain its morphogenetic function.

Our findings suggest that RIPOR2 affects autophagy following the treatment of hair cells with AGs. The mechanisms by which RIPOR2 acts will need further studies. So far, a role for RIPOR2 in autophagy has not been described. As one possibility, RIPOR2 might be required to regulate the normal function of the autophagy pathway that is necessary to maintain cellular homeostasis. This model is consistent with the finding that RIPOR2 binds to GABARAP, suggesting that the two proteins might be part of a protein complex critical for autophagy regulation. Alternatively, the interaction of RIPOR2 with GABARAP might be a pathophysiological response by which RIPOR2 affects the normal biochemical function of GABARAP, and possibly of other proteins, in hair cells, thus leading to the deregulation of a molecular pathway critical for hair cell maintenance, function and survival.

It has been reported previously that AG exposure activates autophagy in hair cells (He et al., 2017; Kim et al., 2017). However, the role of autophagy in AG ototoxicity is controversial and conclusions were largely based on studies using pharmacological inhibitors and

activators of autophagy (Draf et al., 2021; He et al., 2017). For instance, rapamycin, an autophagy activator, was reported to protect hair cells against AG ototoxicity (He *et al.*, 2017); however, in a large-scale unbiased screening, Dr. Ryan's team observed that many compounds that protected hair cells from AG damage are predicted to inhibit autophagy, and some compounds are predicted to enhance autophagy (Draf *et al.*, 2021). The small molecules used in those studies might have complex effects and target other cellular pathways as well (Draf et al., 2021). Rapamycin, for example, inhibits the mammalian target of rapamycin complex 1 (mTORC1), which regulates cell growth and metabolism, and damages hair cells dose-dependently (Leitmeyer et al., 2015; Li et al., 2014). In contrast, our results are based on phenotyping genetically modified mice with defined lesions affecting essential components of the autophagy/mitophagy pathway. Reduced expression of RIPOR2, key autophagy proteins, such as GABARAP or LC3β, and mitophagy proteins, such as PINK1 or Parkin, completely prevents AG ototoxicity. As one possibility, effects of autophagy on hair cell function and survival might be complex, where levels of autophagy/mitophagy need to be finely tuned. Consistent with this finding, we observed that reducing the expression levels of RIPOR2, GABARAP, PINK1 or Parkin was already sufficient to provide significant protective effects. The generation of ROS is presumed to be a major mechanism of AG ototoxicity (Clerici et al., 1995; Hirose et al., 1997), that might trigger the autophagy pathway. However, depletion of cellular antioxidants does not enhance AG-induced hair cell death, suggesting the involvement of other undiscovered molecular processes (Majumder et al., 2015). In addition, the relationship between mitophagy and ROS production is complex. Mitophagy protects cell from ROS stress in some experimental paradigms by eliminating defective or damaged mitochondria. In other paradigms, aberrant activation of mitophagy results in a lethal elevation in ROS production and consequent cell death (Schofield and Schafer, 2021). We observed that increasing intracellular ROS levels or pretreatment with antioxidants had no effect on RIPOR2 translocation, suggesting that the rapid translocation of RIPOR2 triggered by AGs is most likely not caused by an increase in intracellular ROS levels. However, further studies are necessary to elucidate the extent to which ROS might act downstream of RIPOR2 to induce hair cell dysfunction and death. Our studies open the door to analyze the mechanistic details of the interplay between RIPOR2, autophagy/mitophagy and ROS production using molecular tools and genetically modified mice.

Our studies suggest that RIPOR2, GABARAP, LC3β, PINK1 and Parkin are potential targets for preventing AG-induced hearing loss. AGs also exhibit strong vestibulotoxicity and nephrotoxicity. Many of these proteins, identified in this study, are expressed in vestibular hair cells and kidney cells (Orvis et al., 2021; Scheffer et al., 2015). Further studies will systematically investigate the expression profile and localization of these proteins in the vestibule and kidney, as well as the extent to which mitophagy is involved in AG-induced vestibulotoxicity and nephrotoxicity. In addition, not all patients receiving AG treatment suffer from hearing loss. Our studies suggest that it might be worthwhile to analyze the extent to which mutations or polymorphisms in *Ripor2* and genes linked to autophagy/mitophagy might be correlated with sensitivity to AG treatment. This might allow to stratify patients and identify those that are at greatest risk to suffer the negative side effects on auditory function associated with AG treatment.

Limitations of the study

The interaction between RIPOR2 and GEN was detected by immunoblot analysis, but not initially by LC-MS/MS. Future crystallization studies will provide detailed structural insights on this interaction. We have so far observed robust transient translocation of RIPOR2 in organ culture but not *in vivo* following systemic AG administation. One possible reason is that the rapid translocation of RIPOR2 makes it extremely difficult to find the optimal time point for capturing RIPOR2 translocation *in vivo*. Another reason is that the antibody used for immunostaining is not sensentive enough to detect a small amount of translocated RIPOR2 *in vivo*, as the concentration of AGs in the inner ear endolymph is lower than the concentration used *in vitro* (Tran Ba Huy et al., 1986). Regardless, our genetic data clearly demonstrate that RIPOR2 is crucial for the regulation of hair cell death following AG administration.

STAR METHODS

RESOURCE AVAILABILITY

Lead contact—Requests for reagents and resource sharing should be directed to and will be fulfilled by the Lead Contact, Bo Zhao (zhaozb@iu.edu).

Materials availability—Plasmids, antibodies and mouse lines generated in this study are available from the lead contact upon request.

Data and code availability—All original data reported in this paper will be shared by the lead contact upon request.

This paper does not report original code.

Any additional information required to reanalyze the data reported in this paper is available from the lead contact upon request.

EXPERIMENTAL MODEL and SUBJECT DETAILS

Cell culture—HEK293 cells were obtained from the ATCC and maintained in DMEM (ThermoFisher Scientific) supplemented with 10% heat-inactivated fetal bovine serum (Fisher Scientific). HEK293 cells were grown at 37°C in a 5% CO_2 humidified atmosphere. HEI-OC1 cells were provided by Dr. Federico Kalinec and maintained in DMEM supplemented with 10% heat-inactivated fetal bovine serum. HEI-OC1 cells were grown at 33°C in a 10% CO_2 humidified atmosphere.

Animal Models and Animal Care—*Ripor2*$^{-/-}$ (MGI:5085529), *Tmie*$^{-/-}$ (MGI:5784557) and *Grxcr2*$^{-/-}$ (MGI:6281113) mice have been described previously (Liu et al., 2018; Zhao et al., 2014; Zhao et al., 2016). *Gabarap*$^{-/-}$ mouse (B6;129S5-*Gabarap*$^{Gt(OST28330)Lex}$/Mmucd; MGI:3530477) was obtained from Mutant Mouse Resource & Research Centers (MMRRC). *LC3β*$^{-/-}$ mouse (*Map1lc3b*^{tm1Mrab}; MGI:3774111), *Pink1*$^{-/-}$ mouse (B6.129S4-*Pink1*^{tm1Shn}/J; MGI:3716083) and *Prkn*$^{-/-}$ mouse (B6.129S4-*Prkn*^{tm1Shn}/J; MGI:2681404) were obtained from The Jackson Laboratory (Cann et al., 2008; Goldberg et al., 2003; Kitada et al., 2007). To genotype *Ripor2*$^{-/-}$

mice, the following primers were used: 5'- TTAGGCTTAGGAGCCCTGTG -3', 5'- TATCAGCTCTCCAGAGGCAGTC -3', 5'- GGTAAACTGGCTCGGATTAGGG -3' and 5'- TTGACTGTAGCGGCTGATGTTG -3'. To genotype *Tmie*$^{-/-}$ mice, the following primers were used: 5'- GGCTCGGTATCTACAGCGAAAGGCGGCC -3' and 5'- TGCCTGGCTCTGACTAGTTTCTGCAC -3'. To genotype *Grxcr2*$^{-/-}$ mice, the following primers were used: 5'- TCTTCCTACAGTGGCCGAGT -3' and 5'- TGAATGTGAGCGAGATACCG -3'. To genotype *Gabarap*$^{-/-}$ mice, the following primers were used: 5'- ACTTGATACTGCTGCCTCGG -3', 5'- CCTCATCCTGAATGGTGACA -3' and 5'- CCTTGCAAAATGGCGTTACT -3'. To genotype *LC3β*$^{-/-}$ mice, the following primers were used: 5'- GACACCTGTACACTCTGATGCACT -3', 5'- CCTGCCGTCTGCTCTAAGCTG -3' and 5'- CCACTCCCACTGTCCTTTCCTAAT -3'. To genotype *Pink1*$^{-/-}$ mice, the following primers were used: 5'- TCGAGGGACCTAATAACTTCG -3', 5'- GCGGCGACTCTGCTCTATAC -3' and 5'- GCCATATCCACTGCAGGTCT -3'. To genotype *Prkn*$^{-/-}$ mice, the following primers were used: 5'- CCTACACAGAACTGTGACCTGG -3', 5'- GCAGAATTACAGCAGTTACCTGG -3' and 5'- ATGTTGCCGTCCTCCTTGAAGTCG -3'. Both male and female mice were used in our experiments. We did not find any sex-based differences. Mice were maintained on a 12 h day/night cycle with adequate food and water under specific pathogen-free conditions. All animal experiments were carried out in accordance with the National Institutes of Health Guide and were approved by the Institutional Animal Care and Use Committee of Indiana University School of Medicine.

METHOD DETAILS

Cochlear explant culture and immunostaining—Cochlear explants were dissected and cultured in DMEM/F12 media for 4–12 hours at 37 °C in a 5% CO_2 humidified atmosphere. Then, cochlear explants were treated with 1 mM AGs at 37 °C for 2.5, 5, 15, 30, 60, or 120 minutes. Samples were fixed in a fixative containing 4% PFA in Hank's Balanced Salt Solution (HBSS) for 20 min. The tectorial membrane was removed after being washed in HBSS. Samples were blocked at room temperature for 20 minutes with HBSS containing 5% bovine serum albumin (BSA) and 0.5% Triton X-100, and then incubated overnight at 4 °C with primary antibodies in HBSS containing 1% BSA. Tissues were washed in HBSS and incubated with secondary antibodies for 2 hours at room temperature. Then, tissues were mounted in ProLong® Antifade Reagents (ThermoFisher Sci). Stacked images were captured by a DM6 FS automated deconvolution microscope (Leica) using a 100 X objective (HCX PL APO 100x/1.40–0.70 OIL). Depending on the orientation of the samples, 1–4 images were stacked from the base of stereocilia to pericuticular areas, and ImageJ (NIH) was used to measure the fluorescence intensity of RIPOR2.

To raise antibodies against RIPOR2, two peptides (N-SVVEAIPEFHKKLS-C and N-YRSVHPEARGHLSE-C) designed from the primary sequence of mouse RIPOR2 were covalently linked to KLH and injected into New Zealand rabbits (Covance). Following that, antibodies were obtained using affinity purification. The other primary antibodies employed in this study were as follows: anti-GRXCR2 (Cat# HPA059421, Sigma); anti-taperin (Cat# HPA020899, Sigma); anti-CLIC5 (Cat# ACL-025, Alomone Labs); anti-GABARAP (Simons et al., 2019) and anti-GEN (QED Bioscience, Inc). Additional reagents included:

Alexa Fluor 488-phalloidin (ThermoFisher Sci), Alexa Fluor 568-phalloidin (ThermoFisher Sci), Alexa Fluor 488 goat anti-rabbit (ThermoFisher Sci), Alexa Fluor 546 goat anti-rabbit (ThermoFisher Sci), Alexa Fluor 488 goat anti-rat (ThermoFisher Sci) and Alexa Fluor 546 goat anti-rat (ThermoFisher Sci).

Yeast two-hybrid Screening—A cochlear specific yeast two-hybrid cDNA library, suitable for soluble proteins, was constructed previously using mRNA obtained from P3-P7 mouse organ of Corti (Zhao et al., 2014; Zhao et al., 2016). The yeast two-hybrid screening was performed according to the manufacturer's instructions (Dualsystems Biotech). In brief, the *Ripor2* cDNA was cloned into a yeast two-hybrid bait vector and transformed into yeast. The bait's self-activation was evaluated, and the screening stringency was optimized. After that, yeast libraries were transformed into yeast that expressed the bait. Putative interactors were selected from more than 2 million transformants. Positive clones were picked and re-tested for bait dependency. Plasmids from positive clones were isolated and DNA sequencing was used to determine the identity of interaction partners.

GEN pull-down and western blotting—Conjugation of GEN to Sepharose beads was performed according to the published protocol (Karasawa et al., 2010). HEK293 cells or HEI-OC1 cells were lysed in ice-cold RIPA buffer and precleared with empty beads. The lysate was then incubated with the GEN-conjugated beads for 4–6 hours at 4 °C. After being thoroughly washed three times with ice-cold RIPA, beads were collected and LC-MS/MS was performed at The Center for Proteome Analysis at Indiana University School of Medicine. Western blotting was performed as previously described (Liu et al., 2018). All experiments were performed at least 3 times to ensure that the data were reproducible. The following antibodies were used for the experiments: anti-RIPOR2 (rabbit, affinity purified); anti-GABARAP (Cat# AP1821a-ev, Abgent); anti-LC3β (Cat# ab51520, Abcam); anti-α-tubulin (Cat# T6199, Sigma) and anti-HA (Cat# 2367S, Cell Signaling).

Plasmids and Co-IP—The coding sequence of *Ripor2, Grxcr2, taperin, Gabarap, Gabarapl1 and Map1lc3b* were amplified from mouse cochlear cDNA library. Expression of the constructs, immunoprecipitations, and western blots were carried out as described (Li et al., 2021; Liu *et al.*, 2018). Immunoprecipitation experiments were carried out at least 3 times to verify the reproducibility of the data. The following antibodies were used for the experiments: anti-HA (Cat# 2367S, Cell signaling); anti-GFP (Cat# sc-9996, Santa Cruz).

LacZ staining—LacZ staining was carried out as described previously (Zhao et al., 2016). In brief, cochlear whole mounts were fixed in PBS containing 1% PFA, 0.2 % glutaraldehyde, 0.02% NP40 and 0.01% sodium deoxycholate for 15 minutes at room temperature. After being washed 3 times in PBS containing 0.02% NP40 and 0.01% sodium deoxycholate, samples were stained overnight at 37°C in a solution containing 25 mM potassium ferricyanide, 25 mM potassium ferrocyanide, 2 mM $MgCl_2$ and 1 mg/ml X-Gal. Samples were washed 3 times in PBS for a total of 1 hour and then post-fixed overnight at 4°C in 4% PFA. Samples were washed in distilled water and mounted.

Live cell imaging and GTTR uptake assay—Mitodye labeling was performed according to the manufacturer's instructions (Dojindo Laboratories). Stacked Images were

captured by a DM6 FS automated deconvolution microscope (Leica) using a 63 X objective (HCX APO L63x/0.90 water immersion). The wavelengths of the excitation and emission lights were 500–560 and 670–730 nm, respectively. DAPGreen labeling and MT-1 labeling were performed according to the manufacturer's instructions (Dojindo Laboratories). To image DAPGreen signal, the excitation and emission light wavelengths were ~488 nm and 500–563 nm respectively, while to image MT-1 signal, they were ~560 nm and 570–640 nm respectively. GEN was conjugated with Texas Red according to the published protocol (Dai and Steyger, 2008). GTTR uptake assay was performed according to the published protocol (Vu et al., 2013). Images were captured by Leica deconvolution microscope using Rhodamine Red-compatible settings (excitation ~560 nm and emission ~590 nm).

Purification of RIPOR2 protein—Strep-RIPOR2–6XHis, MBP-GRXCR1 and MBP proteins were purified as previously described (Liu and Zhao, 2021). Briefly, pET28a plasmid containing a 6XHis tag was inserted with mouse *Ripor2* cDNA fused with Strep-tag II at the N terminus. *Escherichia coli* BL21 (DE3) cells were cultured in LB liquid medium. The expression of fusion protein was induced overnight at room temperature with 1 mM isopropylthio-β-galactoside. Then cells were harvested and resuspended in a buffer containing 50 mM NaH_2PO_4 (pH 8.0) and 125 mM NaCl. After sonication, the lysate was centrifuged for 30 min at 15,000 rpm. The supernatant was incubated with Ni-NTA resin, and then protein was eluted in an elution buffer containing 250 mM imidazole. To improve the purity, the eluted protein was then incubated with Strep-Tactin® Sepharose® resin and eluted by an elution buffer containing 2.5 mM Desthiobiotin. The purified protein was subsequently dialyzed against PBS buffer.

Kanamycin administration—KAN was dissolved in 0.9% NaCl and then adjusted to a concentration of 80 mg/ml. Subcutaneous injections were administered twice daily for 14 days using a 1 ml syringe with a 27-gauge needle. The first injection was administered around 10 a.m., and the second was administered 8 hours later. The administered dose of KAN was adjusted based on the body weight of animals, which was monitored before injection.

Scanning electron microscopy—The experiment was performed as described (Liu et al., 2018; Zhao et al., 2014; Zhao et al., 2016). In brief, inner ears were dissected and fixed in fixative (2.5% glutaraldehyde; 4% formaldehyde; 0.05 mM Hepes Buffer pH 7.2; 10 mM $CaCl_2$; 5 mM $MgCl_2$; 0.9% NaCl) for 1 hour at room temperature. The stria vascularis, Reissner's membrane and tectorial membrane were then removed from the samples. The samples were post-fixed for 1 day at 4°C in the same fixative and then washed with washing buffer (0.05 mM Hepes Buffer pH 7.2; 0.9% NaCl). After 1 hour of fixation in 1% OsO_4, samples were serially dehydrated in ethanol, dried in a critical point drier (Autosamdri-815A, Tousimis), finely dissected, and mounted on aluminum stubs. Following that, samples were coated with gold and viewed using a JEOL 7800F scanning electron microscope. The percentage of surviving hair cells in the middle turn of cochlea was counted and quantified to determine hair cell survival following KAN treatment.

ABR measurement—ABR recordings were performed as previously described, using the TDT Bioacoustic system 3 (BioSig) (Liu et al., 2018). In brief, mice were anesthetized using a xylazine/ketamine cocktail. Electrodes were placed under the skin at the vertex and ipsilateral ear, while a ground was inserted under the skin near the tail. The speaker was positioned 5 cm away from the mouse's ear. The sound stimulus intensity was started at 90 dB SPL and gradually decreased to a sub-threshold level. ABR thresholds were analyzed for a range of frequencies (for Pure Tone, 4–32 kHz). If no ABR wave was detected during stimulation at maximum strength, a nominal threshold of 90 dB was assigned. Both male and female mice were used in our experiment, and no sex-based difference was detected.

QUANTIFICATION AND STATISTICAL ANALYSIS

Data analysis—We analyzed wild-type and genetically modified mice and used at least three different animals from different litters for each experiment. Precise numbers, sample size, repetitions and statistic tests are indicated in the figures and figure legends. Data in Figure 1E are shown as the mean ± standard deviation (SD) and all of the other data in this study are shown as the mean ± standard error of the mean (SE). The Kolmogorov-Smirnov test was used first to determine the normality of the data distribution. Then Student's two-tailed unpaired t test or two-way ANOVA were used to determine statistical significance (*, $p<0.05$, **, $p<0.01$, ***, $p<0.001$).

Supplementary Material

Refer to Web version on PubMed Central for supplementary material.

ACKNOWLEDGEMENTS

We thank Dr. Federico Kalinec for providing HEI-OC1 cells. We thank Drs. Regina Feederle, Andrew Flatley and Silke Hoffmann for providing GABARAP antibody. This work was supported by National Institute on Deafness and Other Communication Disorders (NIDCD) grant DC017147 (B. Z.), DC018785 (B. Z.), DC005965 (U. M.) and Indiana University School of Medicine startup funding (B. Z.).

REFERENCES

Alharazneh A, Luk L, Huth M, Monfared A, Steyger PS, Cheng AG, and Ricci AJ (2011). Functional hair cell mechanotransducer channels are required for aminoglycoside ototoxicity. PloS one 6, e22347. 10.1371/journal.pone.0022347. [PubMed: 21818312]

Avenarius MR, Jung JY, Askew C, Jones SM, Hunker KL, Azaiez H, Rehman AU, Schraders M, Najmabadi H, Kremer H, et al. (2018). Grxcr2 is required for stereocilia morphogenesis in the cochlea. PloS one 13, e0201713. 10.1371/journal.pone.0201713. [PubMed: 30157177]

Beurg M, Fettiplace R, Nam JH, and Ricci AJ (2009). Localization of inner hair cell mechanotransducer channels using high-speed calcium imaging. Nature neuroscience 12, 553–558. 10.1038/nn.2295. [PubMed: 19330002]

Cann GM, Guignabert C, Ying L, Deshpande N, Bekker JM, Wang L, Zhou B, and Rabinovitch M (2008). Developmental expression of LC3alpha and beta: absence of fibronectin or autophagy phenotype in LC3beta knockout mice. Developmental dynamics : an official publication of the American Association of Anatomists 237, 187–195. 10.1002/dvdy.21392. [PubMed: 18069693]

Clerici WJ, DiMartino DL, and Prasad MR (1995). Direct effects of reactive oxygen species on cochlear outer hair cell shape in vitro. Hearing research 84, 30–40. 10.1016/0378-5955(95)00010-2. [PubMed: 7642453]

Cunningham CL, Qiu X, Wu Z, Zhao B, Peng G, Kim YH, Lauer A, and Muller U (2020). TMIE Defines Pore and Gating Properties of the Mechanotransduction Channel of Mammalian Cochlear Hair Cells. Neuron 107, 126–143 e128. 10.1016/j.neuron.2020.03.033. [PubMed: 32343945]

Cyr JL, Dumont RA, and Gillespie PG (2002). Myosin-1c interacts with hair-cell receptors through its calmodulin-binding IQ domains. The Journal of neuroscience : the official journal of the Society for Neuroscience 22, 2487–2495. . [PubMed: 11923413]

Dai CF, and Steyger PS (2008). A systemic gentamicin pathway across the stria vascularis. Hearing research 235, 114–124. 10.1016/j.heares.2007.10.010. [PubMed: 18082985]

de Bruijn SE, Smits JJ, Liu C, Lanting CP, Beynon AJ, Blankevoort J, Oostrik J, Koole W, de Vrieze E, Cremers C, et al. (2020). A RIPOR2 in-frame deletion is a frequent and highly penetrant cause of adult-onset hearing loss. Journal of medical genetics. 10.1136/jmedgenet-2020-106863.

Dehne N, Rauen U, de Groot H, and Lautermann J (2002). Involvement of the mitochondrial permeability transition in gentamicin ototoxicity. Hearing research 169, 47–55. 10.1016/s0378-5955(02)00338-6. [PubMed: 12121739]

Delmaghani S, Defourny J, Aghaie A, Beurg M, Dulon D, Thelen N, Perfettini I, Zelles T, Aller M, Meyer A, et al. (2015). Hypervulnerability to Sound Exposure through Impaired Adaptive Proliferation of Peroxisomes. Cell 163, 894–906. 10.1016/j.cell.2015.10.023. [PubMed: 26544938]

Diaz-Horta O, Abad C, Cengiz FB, Bademci G, Blackwelder P, Walz K, and Tekin M (2018). Ripor2 is involved in auditory hair cell stereociliary bundle structure and orientation. Journal of molecular medicine 96, 1227–1238. 10.1007/s00109-018-1694-x. [PubMed: 30280293]

Diaz-Horta O, Subasioglu-Uzak A, Grati M, DeSmidt A, Foster J 2nd, Cao L, Bademci G, Tokgoz-Yilmaz S, Duman D, Cengiz FB, et al. (2014). FAM65B is a membrane-associated protein of hair cell stereocilia required for hearing. Proceedings of the National Academy of Sciences of the United States of America 111, 9864–9868. 10.1073/pnas.1401950111. [PubMed: 24958875]

Draf C, Wyrick T, Chavez E, Pak K, Kurabi A, Leichtle A, Dazert S, and Ryan AF (2021). A Screen of Autophagy Compounds Implicates the Proteasome in Mammalian Aminoglycoside-Induced Hair Cell Damage. Frontiers in cell and developmental biology 9, 762751. 10.3389/fcell.2021.762751. [PubMed: 34765606]

Eiyama A, and Okamoto K (2015). PINK1/Parkin-mediated mitophagy in mammalian cells. Current opinion in cell biology 33, 95–101. 10.1016/j.ceb.2015.01.002. [PubMed: 25697963]

Elmore SP, Qian T, Grissom SF, and Lemasters JJ (2001). The mitochondrial permeability transition initiates autophagy in rat hepatocytes. FASEB journal : official publication of the Federation of American Societies for Experimental Biology 15, 2286–2287. 10.1096/fj.01-0206fje. [PubMed: 11511528]

Fausti SA, Henry JA, Schaffer HI, Olson DJ, Frey RH, and McDonald WJ (1992). High-frequency audiometric monitoring for early detection of aminoglycoside ototoxicity. The Journal of infectious diseases 165, 1026–1032. 10.1093/infdis/165.6.1026. [PubMed: 1583319]

Francis SP, Katz J, Fanning KD, Harris KA, Nicholas BD, Lacy M, Pagana J, Agris PF, and Shin JB (2013). A novel role of cytosolic protein synthesis inhibition in aminoglycoside ototoxicity. The Journal of neuroscience : the official journal of the Society for Neuroscience 33, 3079–3093. 10.1523/JNEUROSCI.3430-12.2013. [PubMed: 23407963]

Gagnon LH, Longo-Guess CM, Berryman M, Shin JB, Saylor KW, Yu H, Gillespie PG, and Johnson KR (2006). The chloride intracellular channel protein CLIC5 is expressed at high levels in hair cell stereocilia and is essential for normal inner ear function. The Journal of neuroscience : the official journal of the Society for Neuroscience 26, 10188–10198. 10.1523/JNEUROSCI.2166-06.2006. [PubMed: 17021174]

Goldberg MS, Fleming SM, Palacino JJ, Cepeda C, Lam HA, Bhatnagar A, Meloni EG, Wu N, Ackerson LC, Klapstein GJ, et al. (2003). Parkin-deficient mice exhibit nigrostriatal deficits but not loss of dopaminergic neurons. The Journal of biological chemistry 278, 43628–43635. 10.1074/jbc.M308947200. [PubMed: 12930822]

Guan MX (2011). Mitochondrial 12S rRNA mutations associated with aminoglycoside ototoxicity. Mitochondrion 11, 237–245. 10.1016/j.mito.2010.10.006. [PubMed: 21047563]

Hasson T, Gillespie PG, Garcia JA, MacDonald RB, Zhao Y, Yee AG, Mooseker MS, and Corey DP (1997). Unconventional myosins in inner-ear sensory epithelia. The Journal of cell biology 137, 1287–1307. 10.1083/jcb.137.6.1287. [PubMed: 9182663]

He Z, Guo L, Shu Y, Fang Q, Zhou H, Liu Y, Liu D, Lu L, Zhang X, Ding X, et al. (2017). Autophagy protects auditory hair cells against neomycin-induced damage. Autophagy 13, 1884–1904. 10.1080/15548627.2017.1359449. [PubMed: 28968134]

Hirose K, Hockenbery DM, and Rubel EW (1997). Reactive oxygen species in chick hair cells after gentamicin exposure in vitro. Hearing research 104, 1–14. 10.1016/s0378-5955(96)00169-4. [PubMed: 9119753]

Huth ME, Han KH, Sotoudeh K, Hsieh YJ, Effertz T, Vu AA, Verhoeven S, Hsieh MH, Greenhouse R, Cheng AG, and Ricci AJ (2015). Designer aminoglycosides prevent cochlear hair cell loss and hearing loss. The Journal of clinical investigation 125, 583–592. 10.1172/JCI77424. [PubMed: 25555219]

Huth ME, Ricci AJ, and Cheng AG (2011). Mechanisms of aminoglycoside ototoxicity and targets of hair cell protection. International journal of otolaryngology 2011, 937861. 10.1155/2011/937861. [PubMed: 22121370]

Imtiaz A, Kohrman DC, and Naz S (2014). A frameshift mutation in GRXCR2 causes recessively inherited hearing loss. Human mutation 35, 618–624. 10.1002/humu.22545. [PubMed: 24619944]

Iwashita H, Sakurai HT, Nagahora N, Ishiyama M, Shioji K, Sasamoto K, Okuma K, Shimizu S, and Ueno Y (2018). Small fluorescent molecules for monitoring autophagic flux. FEBS Lett 592, 559–567. 10.1002/1873-3468.12979. [PubMed: 29355929]

Kalinec G, Thein P, Park C, and Kalinec F (2016). HEI-OC1 cells as a model for investigating drug cytotoxicity. Hearing research 335, 105–117. 10.1016/j.heares.2016.02.019. [PubMed: 26930622]

Karasawa T, Wang Q, David LL, and Steyger PS (2010). CLIMP-63 is a gentamicin-binding protein that is involved in drug-induced cytotoxicity. Cell death & disease 1, e102. 10.1038/cddis.2010.80. [PubMed: 21368867]

Kim YJ, Tian C, Kim J, Shin B, Choo OS, Kim YS, and Choung YH (2017). Autophagic flux, a possible mechanism for delayed gentamicin-induced ototoxicity. Scientific reports 7, 41356. 10.1038/srep41356. [PubMed: 28145495]

Kitada T, Pisani A, Porter DR, Yamaguchi H, Tscherter A, Martella G, Bonsi P, Zhang C, Pothos EN, and Shen J (2007). Impaired dopamine release and synaptic plasticity in the striatum of PINK1-deficient mice. Proceedings of the National Academy of Sciences of the United States of America 104, 11441–11446. 10.1073/pnas.0702717104. [PubMed: 17563363]

Klionsky DJ, Abdel-Aziz AK, Abdelfatah S, Abdellatif M, Abdoli A, Abel S, Abeliovich H, Abildgaard MH, Abudu YP, Acevedo-Arozena A, et al. (2021). Guidelines for the use and interpretation of assays for monitoring autophagy (4th edition)(1). Autophagy 17, 1–382. 10.1080/15548627.2020.1797280. [PubMed: 33634751]

Klionsky DJ, Abdelmohsen K, Abe A, Abedin MJ, Abeliovich H, Acevedo Arozena A, Adachi H, Adams CM, Adams PD, Adeli K, et al. (2016). Guidelines for the use and interpretation of assays for monitoring autophagy (3rd edition). Autophagy 12, 1–222. 10.1080/15548627.2015.1100356. [PubMed: 26799652]

Krause KM, Serio AW, Kane TR, and Connolly LE (2016). Aminoglycosides: An Overview. Cold Spring Harbor perspectives in medicine 6. 10.1101/cshperspect.a027029.

Leitmeyer K, Glutz A, Radojevic V, Setz C, Huerzeler N, Bumann H, Bodmer D, and Brand Y (2015). Inhibition of mTOR by Rapamycin Results in Auditory Hair Cell Damage and Decreased Spiral Ganglion Neuron Outgrowth and Neurite Formation In Vitro. Biomed Res Int 2015, 925890. 10.1155/2015/925890. [PubMed: 25918725]

Lewis RJ (2004). Sax's dangerous properties of industrial materials (Wiley).

Li H, and Steyger PS (2011). Systemic aminoglycosides are trafficked via endolymph into cochlear hair cells. Scientific reports 1, 159. 10.1038/srep00159. [PubMed: 22355674]

Li J, Kim SG, and Blenis J (2014). Rapamycin: one drug, many effects. Cell metabolism 19, 373–379. 10.1016/j.cmet.2014.01.001. [PubMed: 24508508]

Li J, Liu C, Kaefer S, Youssef M, and Zhao B (2022). The Mechanotransduction Channel and Organic Cation Transporter Are Critical for Cisplatin Ototoxicity in Murine Hair Cells. Front Mol Neurosci 15, 835448. 10.3389/fnmol.2022.835448. [PubMed: 35221917]

Li J, Liu C, and Zhao B (2021). N-Terminus of GRXCR2 Interacts With CLIC5 and Is Essential for Auditory Perception. Frontiers in cell and developmental biology 9, 671364. 10.3389/fcell.2021.671364. [PubMed: 34026762]

Li Y, Pohl E, Boulouiz R, Schraders M, Nurnberg G, Charif M, Admiraal RJ, von Ameln S, Baessmann I, Kandil M, et al. (2010). Mutations in TPRN cause a progressive form of autosomal-recessive nonsyndromic hearing loss. American journal of human genetics 86, 479–484. 10.1016/j.ajhg.2010.02.003. [PubMed: 20170898]

Liu C, Luo N, Tung CY, Perrin BJ, and Zhao B (2018). GRXCR2 Regulates Taperin Localization Critical for Stereocilia Morphology and Hearing. Cell reports 25, 1268–1280 e1264. 10.1016/j.celrep.2018.09.063. [PubMed: 30380417]

Liu C, and Zhao B (2021). Murine GRXCR1 Has a Different Function Than GRXCR2 in the Morphogenesis of Stereocilia. Frontiers in cellular neuroscience 15, 714070. 10.3389/fncel.2021.714070. [PubMed: 34366792]

Majumder P, Duchen MR, and Gale JE (2015). Cellular glutathione content in the organ of Corti and its role during ototoxicity. Frontiers in cellular neuroscience 9, 143. 10.3389/fncel.2015.00143. [PubMed: 25972783]

Marcotti W, van Netten SM, and Kros CJ (2005). The aminoglycoside antibiotic dihydrostreptomycin rapidly enters mouse outer hair cells through the mechano-electrical transducer channels. The Journal of physiology 567, 505–521. 10.1113/jphysiol.2005.085951. [PubMed: 15994187]

Matsui JI, Ogilvie JM, and Warchol ME (2002). Inhibition of caspases prevents ototoxic and ongoing hair cell death. The Journal of neuroscience : the official journal of the Society for Neuroscience 22, 1218–1227. [PubMed: 11850449]

Matt T, Ng CL, Lang K, Sha SH, Akbergenov R, Shcherbakov D, Meyer M, Duscha S, Xie J, Dubbaka SR, et al. (2012). Dissociation of antibacterial activity and aminoglycoside ototoxicity in the 4-monosubstituted 2-deoxystreptamine apramycin. Proceedings of the National Academy of Sciences of the United States of America 109, 10984–10989. 10.1073/pnas.1204073109. [PubMed: 22699498]

Nguyen TN, Padman BS, Usher J, Oorschot V, Ramm G, and Lazarou M (2016). Atg8 family LC3/GABARAP proteins are crucial for autophagosome-lysosome fusion but not autophagosome formation during PINK1/Parkin mitophagy and starvation. The Journal of cell biology 215, 857–874. 10.1083/jcb.201607039. [PubMed: 27864321]

O'Sullivan ME, Perez A, Lin R, Sajjadi A, Ricci AJ, and Cheng AG (2017). Towards the Prevention of Aminoglycoside-Related Hearing Loss. Frontiers in cellular neuroscience 11, 325. 10.3389/fncel.2017.00325. [PubMed: 29093664]

Orvis J, Gottfried B, Kancherla J, Adkins RS, Song Y, Dror AA, Olley D, Rose K, Chrysostomou E, Kelly MC, et al. (2021). gEAR: Gene Expression Analysis Resource portal for community-driven, multi-omic data exploration. Nat Methods 18, 843–844. 10.1038/s41592-021-01200-9. [PubMed: 34172972]

Owens KN, Cunningham DE, MacDonald G, Rubel EW, Raible DW, and Pujol R (2007). Ultrastructural analysis of aminoglycoside-induced hair cell death in the zebrafish lateral line reveals an early mitochondrial response. The Journal of comparative neurology 502, 522–543. 10.1002/cne.21345. [PubMed: 17394157]

Prezant TR, Agapian JV, Bohlman MC, Bu X, Oztas S, Qiu WQ, Arnos KS, Cortopassi GA, Jaber L, Rotter JI, and et al. (1993). Mitochondrial ribosomal RNA mutation associated with both antibiotic-induced and non-syndromic deafness. Nat Genet 4, 289–294. 10.1038/ng0793-289. [PubMed: 7689389]

Rehman AU, Morell RJ, Belyantseva IA, Khan SY, Boger ET, Shahzad M, Ahmed ZM, Riazuddin S, Khan SN, Riazuddin S, and Friedman TB (2010). Targeted capture and next-generation sequencing identifies C9orf75, encoding taperin, as the mutated gene in nonsyndromic deafness DFNB79. American journal of human genetics 86, 378–388. 10.1016/j.ajhg.2010.01.030. [PubMed: 20170899]

Rusch A, Kros CJ, and Richardson GP (1994). Block by amiloride and its derivatives of mechano-electrical transduction in outer hair cells of mouse cochlear cultures. The Journal of physiology 474, 75–86. 10.1113/jphysiol.1994.sp020004. [PubMed: 7516972]

Schaaf MB, Keulers TG, Vooijs MA, and Rouschop KM (2016). LC3/GABARAP family proteins: autophagy-(un)related functions. FASEB journal : official publication of the Federation of American Societies for Experimental Biology 30, 3961–3978. 10.1096/fj.201600698R. [PubMed: 27601442]

Scheffer DI, Shen J, Corey DP, and Chen ZY (2015). Gene Expression by Mouse Inner Ear Hair Cells during Development. The Journal of neuroscience : the official journal of the Society for Neuroscience 35, 6366–6380. 10.1523/JNEUROSCI.5126-14.2015. [PubMed: 25904789]

Schofield JH, and Schafer ZT (2021). Mitochondrial Reactive Oxygen Species and Mitophagy: A Complex and Nuanced Relationship. Antioxidants & redox signaling 34, 517–530. 10.1089/ars.2020.8058. [PubMed: 32079408]

Seco CZ, Oonk AM, Dominguez-Ruiz M, Draaisma JM, Gandia M, Oostrik J, Neveling K, Kunst HP, Hoefsloot LH, del Castillo I, et al. (2015). Progressive hearing loss and vestibular dysfunction caused by a homozygous nonsense mutation in CLIC5. European journal of human genetics : EJHG 23, 189–194. 10.1038/ejhg.2014.83. [PubMed: 24781754]

Simons IM, Mohrluder J, Feederle R, Kremmer E, Zobel T, Dobner J, Bleffert N, Hoffmann S, and Willbold D (2019). The highly GABARAP specific rat monoclonal antibody 8H5 visualizes GABARAP in immunofluorescence imaging at endogenous levels. Scientific reports 9, 526. 10.1038/s41598-018-36717-1. [PubMed: 30679523]

Tao L, and Segil N (2015). Early transcriptional response to aminoglycoside antibiotic suggests alternate pathways leading to apoptosis in sensory hair cells in the mouse inner ear. Frontiers in cellular neuroscience 9, 190. 10.3389/fncel.2015.00190. [PubMed: 26052268]

Thomas AJ, Hailey DW, Stawicki TM, Wu P, Coffin AB, Rubel EW, Raible DW, Simon JA, and Ou HC (2013). Functional mechanotransduction is required for cisplatin-induced hair cell death in the zebrafish lateral line. The Journal of neuroscience : the official journal of the Society for Neuroscience 33, 4405–4414. 10.1523/JNEUROSCI.3940-12.2013. [PubMed: 23467357]

Tran Ba Huy P, Bernard P, and Schacht J (1986). Kinetics of gentamicin uptake and release in the rat. Comparison of inner ear tissues and fluids with other organs. The Journal of clinical investigation 77, 1492–1500. 10.1172/JCI112463. [PubMed: 3700652]

Vaites LP, Paulo JA, Huttlin EL, and Harper JW (2018). Systematic Analysis of Human Cells Lacking ATG8 Proteins Uncovers Roles for GABARAPs and the CCZ1/MON1 Regulator C18orf8/RMC1 in Macroautophagic and Selective Autophagic Flux. Mol Cell Biol 38. 10.1128/MCB.00392-17.

Vu AA, Nadaraja GS, Huth ME, Luk L, Kim J, Chai R, Ricci AJ, and Cheng AG (2013). Integrity and regeneration of mechanotransduction machinery regulate aminoglycoside entry and sensory cell death. PloS one 8, e54794. 10.1371/journal.pone.0054794. [PubMed: 23359017]

Xie W, and Zhou J (2018). Aberrant regulation of autophagy in mammalian diseases. Biology letters 14. 10.1098/rsbl.2017.0540.

Yu J, Zheng J, Zhao X, Liu J, Mao Z, Ling Y, Chen D, Chen C, Hui L, Cui L, et al. (2014). Aminoglycoside stress together with the 12S rRNA 1494C>T mutation leads to mitophagy. PloS one 9, e114650. 10.1371/journal.pone.0114650. [PubMed: 25474306]

Zhao B, Wu Z, Grillet N, Yan L, Xiong W, Harkins-Perry S, and Muller U (2014). TMIE is an essential component of the mechanotransduction machinery of cochlear hair cells. Neuron 84, 954–967. 10.1016/j.neuron.2014.10.041. [PubMed: 25467981]

Zhao B, Wu Z, and Muller U (2016). Murine Fam65b forms ring-like structures at the base of stereocilia critical for mechanosensory hair cell function. eLife 5. 10.7554/eLife.14222.

Zhao Y, Yamoah EN, and Gillespie PG (1996). Regeneration of broken tip links and restoration of mechanical transduction in hair cells. Proceedings of the National Academy of Sciences of the United States of America 93, 15469–15474. 10.1073/pnas.93.26.15469. [PubMed: 8986835]

Highlights

- Dysfunction of autophagy is linked to aminoglycoside-induced hearing loss
- Aminoglycosides trigger rapid translocation of RIPOR2 in hair cells
- RIPOR2 interacts with GABARAP and affects autophagy in hair cells
- Autophagy components may be therapeutic targets to prevent AG ototoxicity

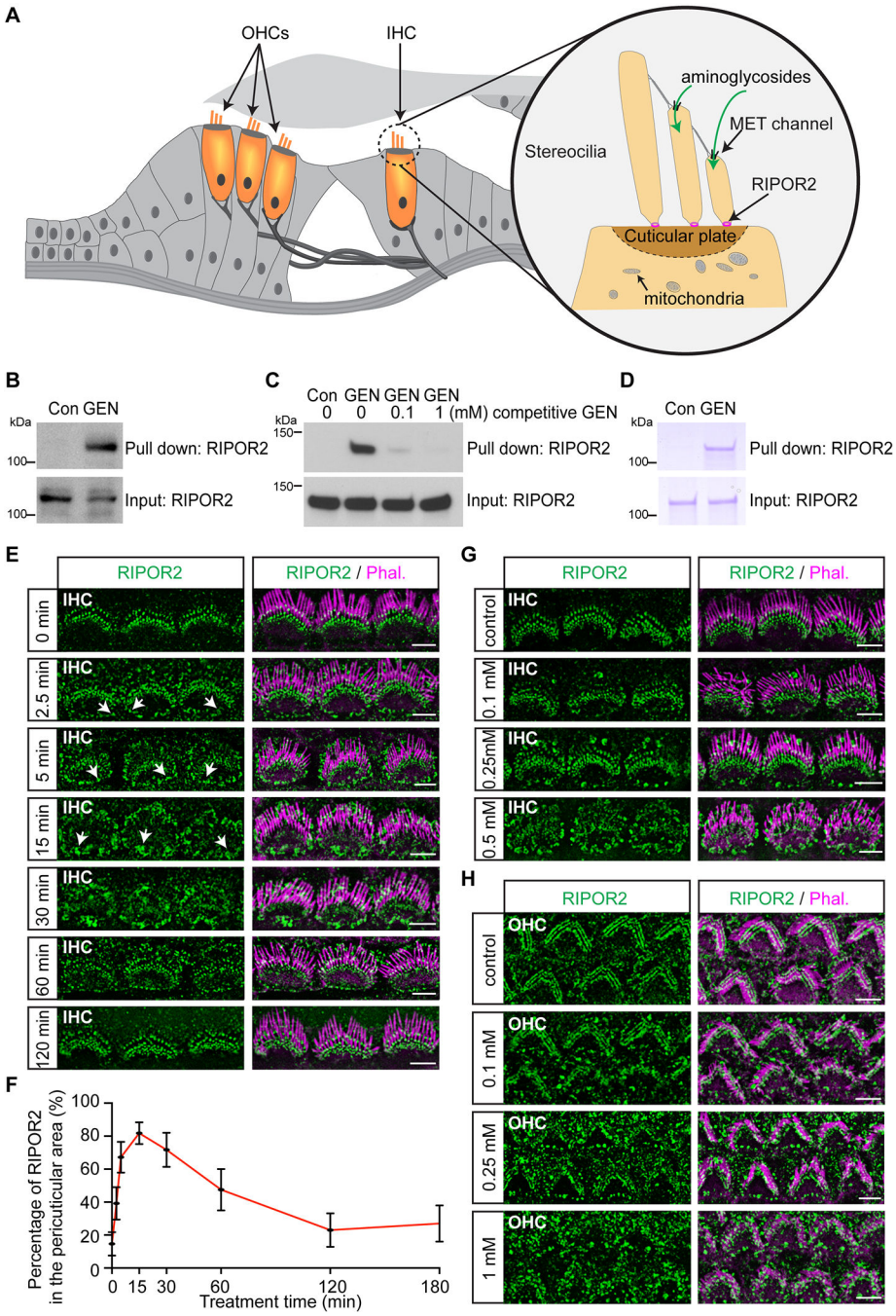

Figure 1: Rapid translocation of RIPOR2 in cochlear hair cells in response to GEN.

(A) Organ of Corti has one row of inner hair cells (IHCs) and three rows of outer hair cells (OHCs). Hair cell stereocilia are organized in rows of decreasing height. The mechanotransduction (MET) channel, localized near the tips of stereocilia, is the major entry route for aminoglycosides to enter hair cells. RIPOR2 forms a circumferential ring structure at the base of each stereocilium. Mitochondria localize beneath the stereocilia and cuticular plate. **(B-D)** GEN pull-down assays were performed using lysates from HEI-OC1 cells (B), HEK293 cells transfected with RIPOR2-GFP (C), or purified 6XHis-tagged RIPOR2 protein

(D). 0.1 mM (lane 3) or 1 mM (lane 4) GEN was added into the cell lysates to competitively block the binding between RIPOR2 and GEN-conjugated beads (C). Molecular weight markers (in kDa) are indicated. **(E)** P4 wild-type cochlear explants were treated with 1 mM GEN for 2.5, 5, 15, 30, 60, or 120 minutes, and stained for RIPOR2 and phalloidin. **(F)** Percentage of RIPOR2 in the pericuticular area, as shown in (E). Data are represented as the mean ± standard deviation. In each group 100 IHCs from at least three mice were analyzed. **(G-H)** P4 wild-type cochlear explants were treated with GEN of different concentrations for 15 minutes. RIPOR2 translocation was detected in IHCs (G) and OHCs (H). All the experiments were repeated at least three times. Scale bars: 5 μm.

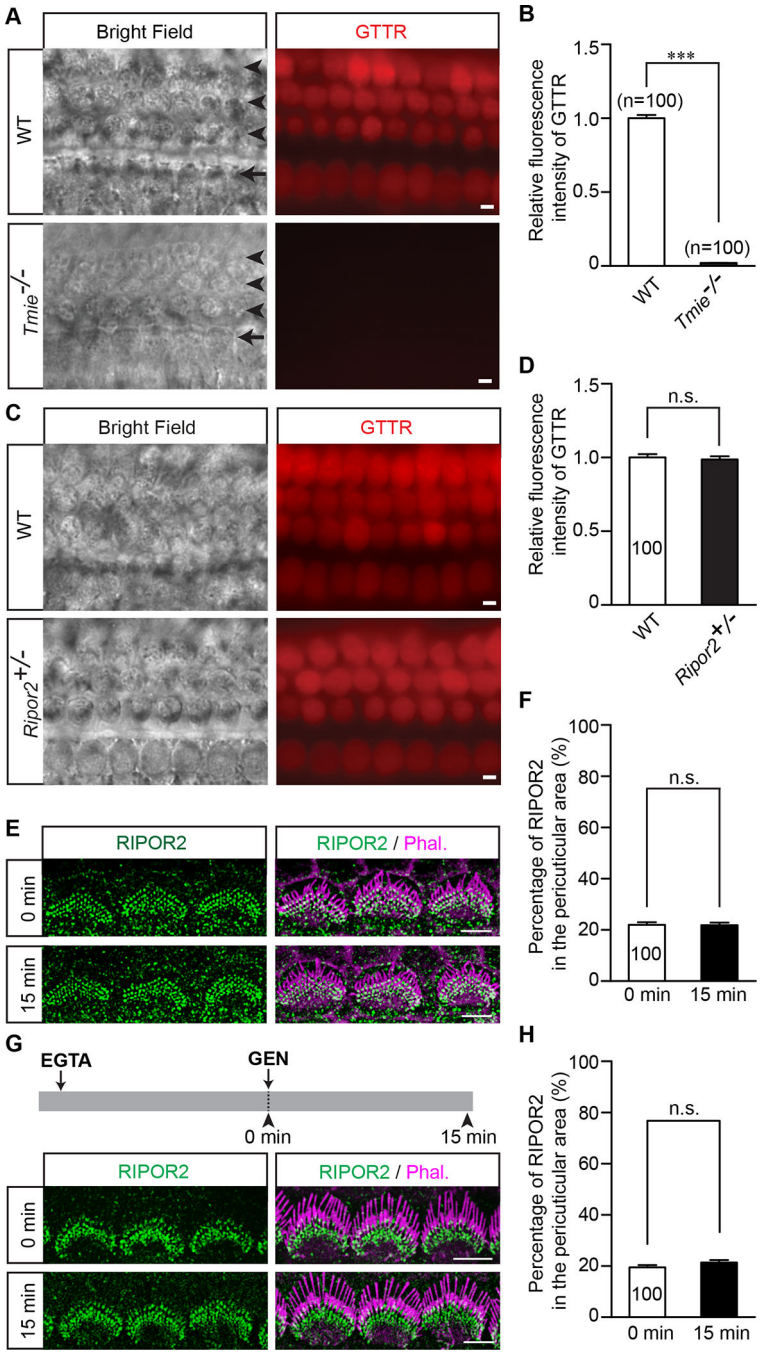

Figure 2: AG-induced RIPOR2 translocation requires AG entry via MET channels.

(A) P4 wild-type and *Tmie*$^{-/-}$ hair cells were treated with GEN-conjugated Texas Red (GTTR) for 15 minutes. Arrowheads, OHCs; arrows, IHCs. **(B)** Quantification of the GTTR fluorescence intensity as shown in (A). **(C)** P4 wild-type and *Ripor2*$^{+/-}$ cochlear explants were treated with GTTR for 15 minutes. **(D)** Quantification of GTTR fluorescence intensity as shown in (C). **(E)** *Tmie*$^{-/-}$ hair cells were treated with 1 mM GEN for 15 minutes, and stained for RIPOR2 and phalloidin. **(F)** Percentage of RIPOR2 in the pericuticular area as shown in (E). **(G)** P4 wild-type hair cells were treated with 5 mM EGTA for 30 minutes

to block the MET, and then treated with 1 mM GEN for 15 minutes. **(H)** Percentage of RIPOR2 in the pericuticular area as shown in (G). All the experiments were repeated at least three times, and in each group 100 IHCs from at least three mice were measured. n.s., not significant, ***$p < 0.001$ by Student's t test. Scale bars: 5 μm.

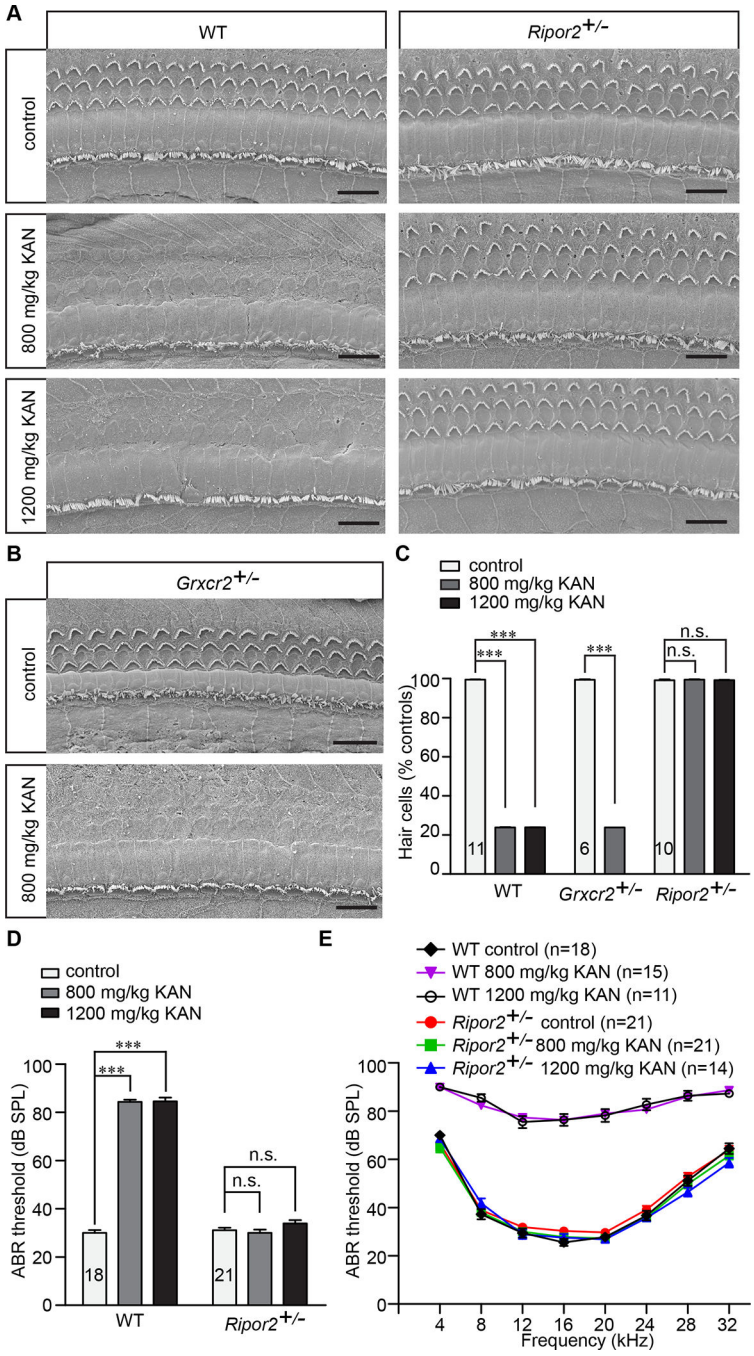

Figure 3. Reducing RIPOR2 expression prevents AG-induced hair cell death and subsequent hearing loss.

(A-B) Wild-type and *Ripor2*$^{+/-}$ mice (A), and *Grxcr2*$^{+/-}$ mice (B) received 800 mg/kg or 1200 mg/kg KAN subcutaneously for 14 days. Middle regions of cochlea were analyzed by scanning electron microscopy. **(C)** Percentage of surviving hair cells. Analyzed mouse numbers are indicated. **(D-E)** ABR thresholds for click stimuli (D) or pure tones (E) in wild-type and *Ripor2*$^{+/-}$ mice following KAN treatment. The experiments were repeated at least three times. Analyzed mouse numbers are indicated. n.s., not significant, ***p < 0.001

by Student's t test (C, D). $p < 0.001$ between saline-treated and KAN-treated wild-type mice; no significant difference between saline-treated and KAN-treated *Ripor2*$^{+/-}$ mice (two-way ANOVA) (E). Scale bars: 10 μm.

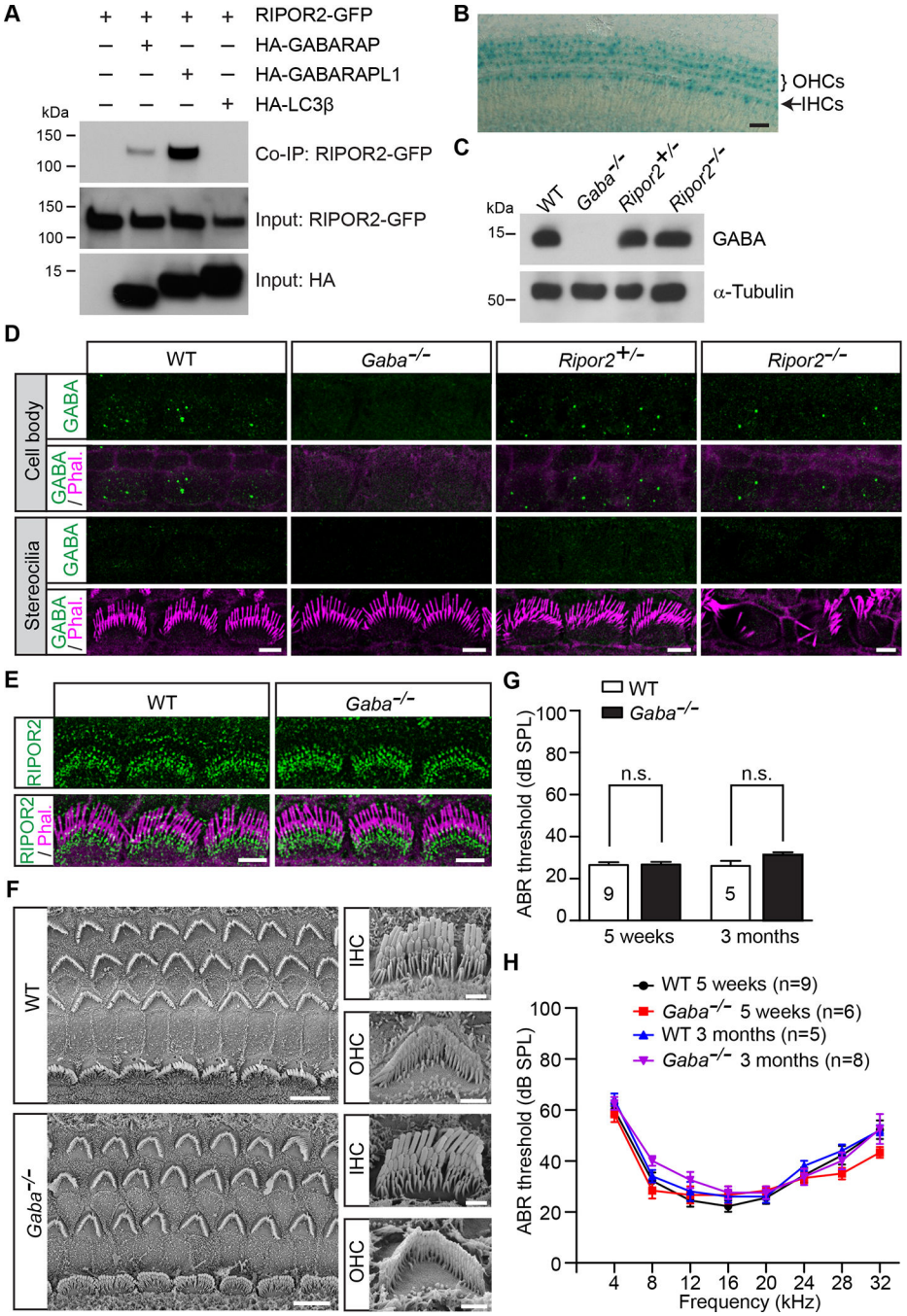

Figure 4. GABARAP interacts with RIPOR2 but is not essential for normal hearing.

(A) HEK293 cells were transfected with the constructs indicated on the top of each panel. Immunoprecipitations were performed using HA-antibody. The upper row shows Co-IP results and lower rows show input proteins. The experiments were repeated at least three times. **(B)** LacZ staining was used to detect *Gabarap* expression in P6 *Gabarap*$^{+/-}$ cochlea. **(C)** Western blotting was used to analyze P7 wild-type, *Gabarap*$^{-/-}$, *Ripor2*$^{+/-}$ and *Ripor2*$^{-/-}$ cochlear samples. The experiments were repeated three times. **(D)** P7 hair cells were stained for GABARAP and phalloidin. Note, GABARAP was punctately distributed in the cell body

in wild-type, *Ripor2*$^{+/-}$ *and Ripor2*$^{+/-}$ hair cells. The signal was disappeared in *Gabarap*$^{-/-}$ hair cells. In each group, more than three mice were used. **(E)** P7 wild-type and *Gabarap*$^{-/-}$ cochlear whole mounts were stained for RIPOR2 and phalloidin. In each group, more than three mice were used. **(F)** Scanning electron microscopy images showing P7 wild-type and *Gabarap*$^{-/-}$ cochlear epithelia. In each group, more than three mice were used. **(G-H)** ABR thresholds for click stimuli (G) or pure tones (H) in 5-week-old and 3-month-old wild-type and *Gabarap*$^{-/-}$ mice. Analyzed mouse numbers are indicated. No significant difference in click ABR thresholds (Student's t test) or pure-tone thresholds (two-way ANOVA) between wild-type and *Gabarap*$^{-/-}$ mice was detected. Scale bars: (B) 20 μm; (D, E) 5 μm; (F) left panel, 5 μm; right panel 1 μm.

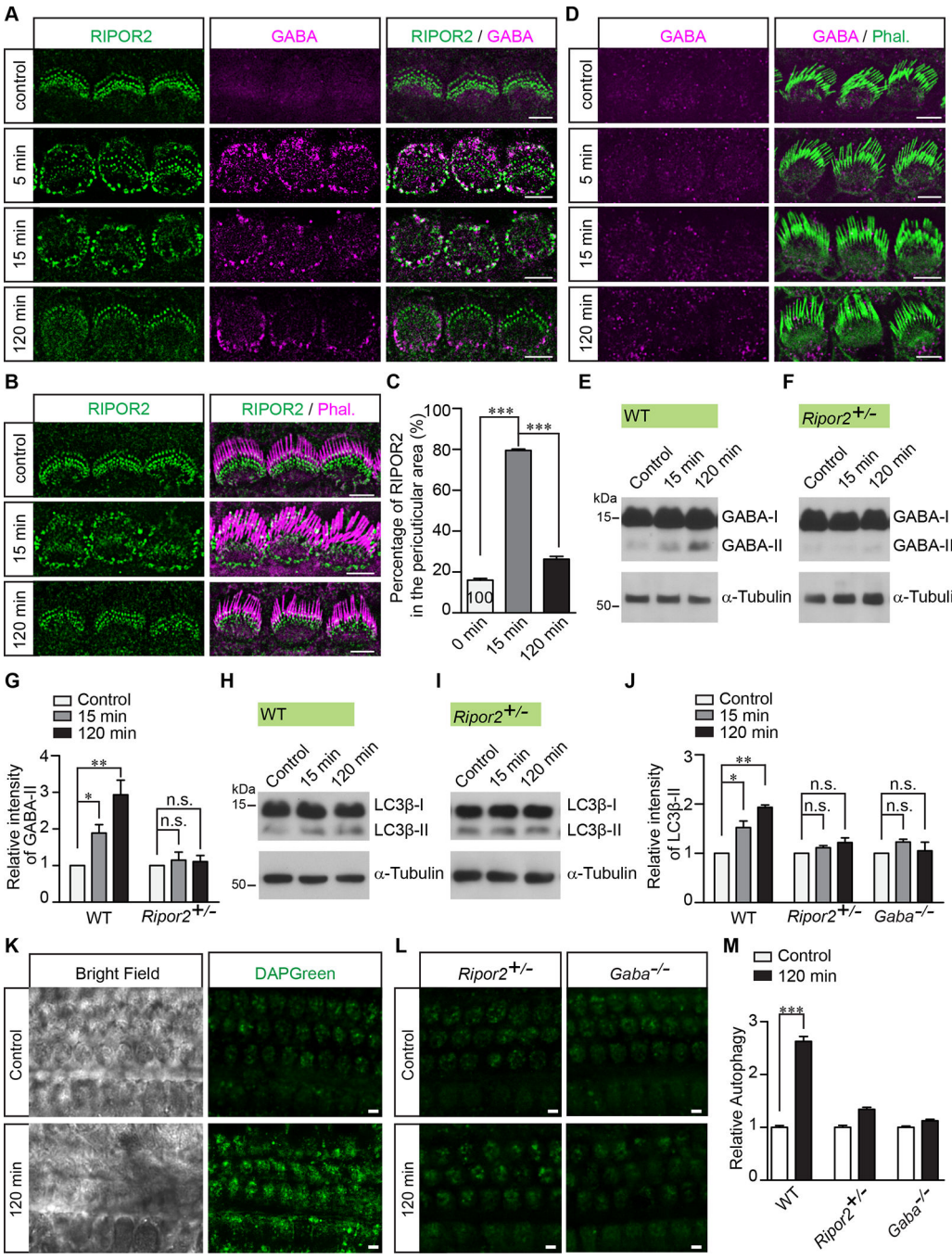

Figure 5. RIPOR2 colocalizes with GABARAP in the pericuticular area and regulates autophagy activation following AG exposure.

(A) P4 wild-type cochlear explants were treated with 1 mM GEN, and stained for RIPOR2 and GABARAP. In each group, more than three mice were used. **(B)** P4 *Gabarap*$^{-/-}$ cochlear explants were treated with 1 mM GEN, and stained for RIPOR2 and phalloidin. In each group, more than three mice were used. **(C)** Percentage of RIPOR2 in the pericuticular area as shown in (B). **(D)** P4 *Ripor2*$^{+/-}$ cochlear explants were treated with 1 mM GEN, and stained for GABARAP and phalloidin. Note, no significant accumulation of GABARAP

was observed in the pericuticular area. In each group, more than three mice were used. **(E-F)** P4 wild-type (E) or *Ripor2*$^{+/-}$ (F) cochlear explants were treated with 1 mM GEN. Western blotting was performed to detect lipidated GABARAP (GABA-II). The experiments were repeated at least three times. **(G)** Quantification of lipidated GABARAP as shown in (E-F). **(H-I)** P4 wild-type (H) or *Ripor2*$^{+/-}$ (I) cochlear explants were treated with 1 mM GEN. Lipidated LC3β (LC3β-II) was detected. The experiments were repeated at least three times. **(J)** Quantification of LC3β-II in wild-type, *Ripor2*$^{+/-}$ and *Gabarap*$^{-/-}$ mice. **(K-L)** P4 wild-type (K), *Ripor2*$^{+/-}$ or *Gabarap*$^{-/-}$ (L) cochlear explants were treated with 1 mM GEN, and labeled with DAPGreen dye. **(M)** Quantification of DAPGreen intensity in wild-type, *Ripor2*$^{+/-}$ and *Gabarap*$^{-/-}$ hair cells. The experiments were repeated at least three times, and in each group more than 100 hair cells from at least three mice were measured. n.s., not significant, *$p < 0.05$, **$p < 0.01$, ***$p < 0.001$ by Student's t test. Scale bars: 5 μm.

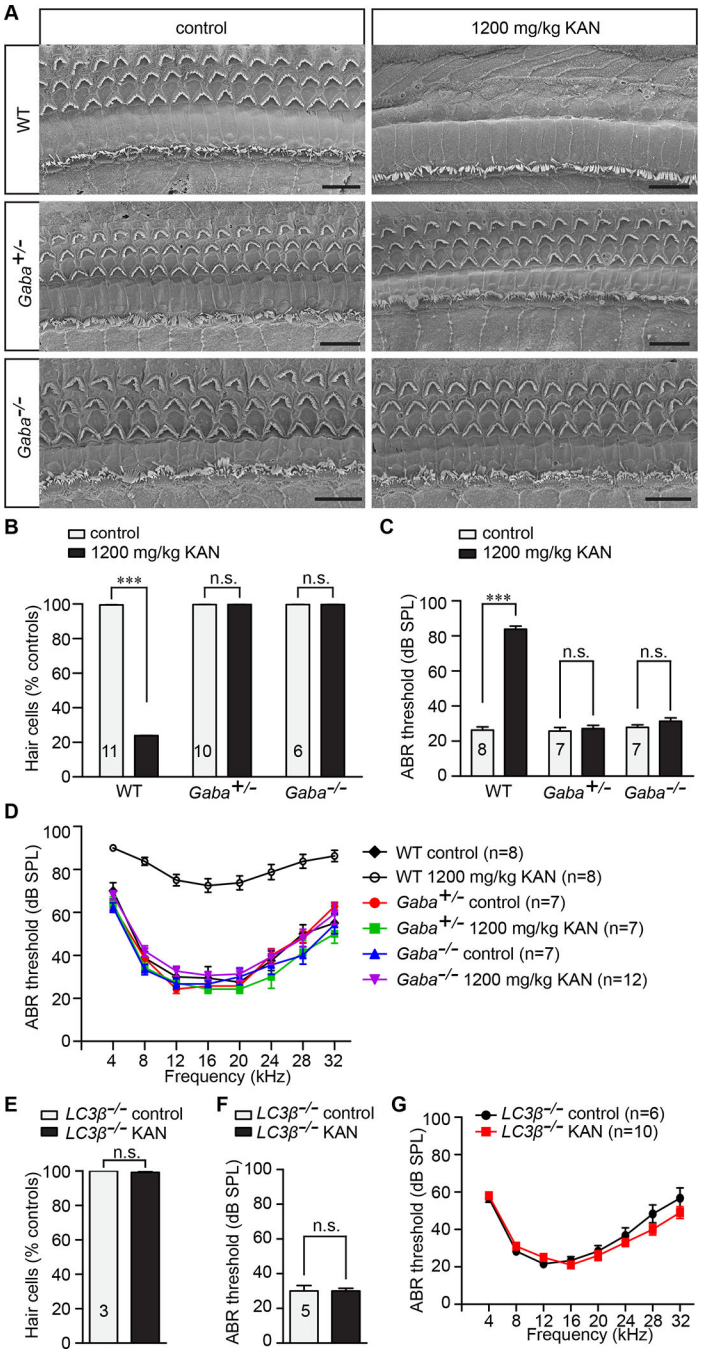

Figure 6. GABARAP and LC3β are required for AG-induced hair cell death and subsequent hearing loss.

(A) Wild-type, *Gabarap*$^{+/-}$ and *Gabarap*$^{-/-}$ mice received 1200 mg/kg KAN for 14 days. Middle regions of cochlea were analyzed by scanning electron microscopy. (B) Quantification of the percentage of surviving hair cells, as shown in (A). Analyzed mouse numbers are indicated. n.s., not significant, ***p < 0.001 by Student's t test. (C-D) ABR thresholds for click stimuli (C) or pure tones (D) in wild-type, *Gabarap*$^{+/-}$ and *Gabarap*$^{-/-}$ mice following KAN treatment. Analyzed mouse numbers are indicated. n.s., not significant, ***p < 0.001 by Student's t test (C). p < 0.001 between KAN-treated and control wild-type

mice; no significant difference between KAN-treated and control *Gabarap*$^{+/-}$ or *Gabarap*$^{-/-}$ mice (two-way ANOVA) (D). (E) Percentage of surviving *LC3β*$^{-/-}$ hair cells following 1200mg/kg KAN treatment. Analyzed mouse numbers are indicated. n.s., not significant by Student's t test. (F-G) *LC3β*$^{-/-}$ mice received 1200 mg/kg KAN for 14 days. ABR thresholds for click stimuli (F) or pure tones (G) in *LC3β*$^{-/-}$ mice were measured. Analyzed mouse numbers are indicated. n.s., not significant by Student's t test (F). No significant difference between KAN-treated and control *LC3β*$^{-/-}$ mice (two-way ANOVA) (G). Scale bars: 10 μm.

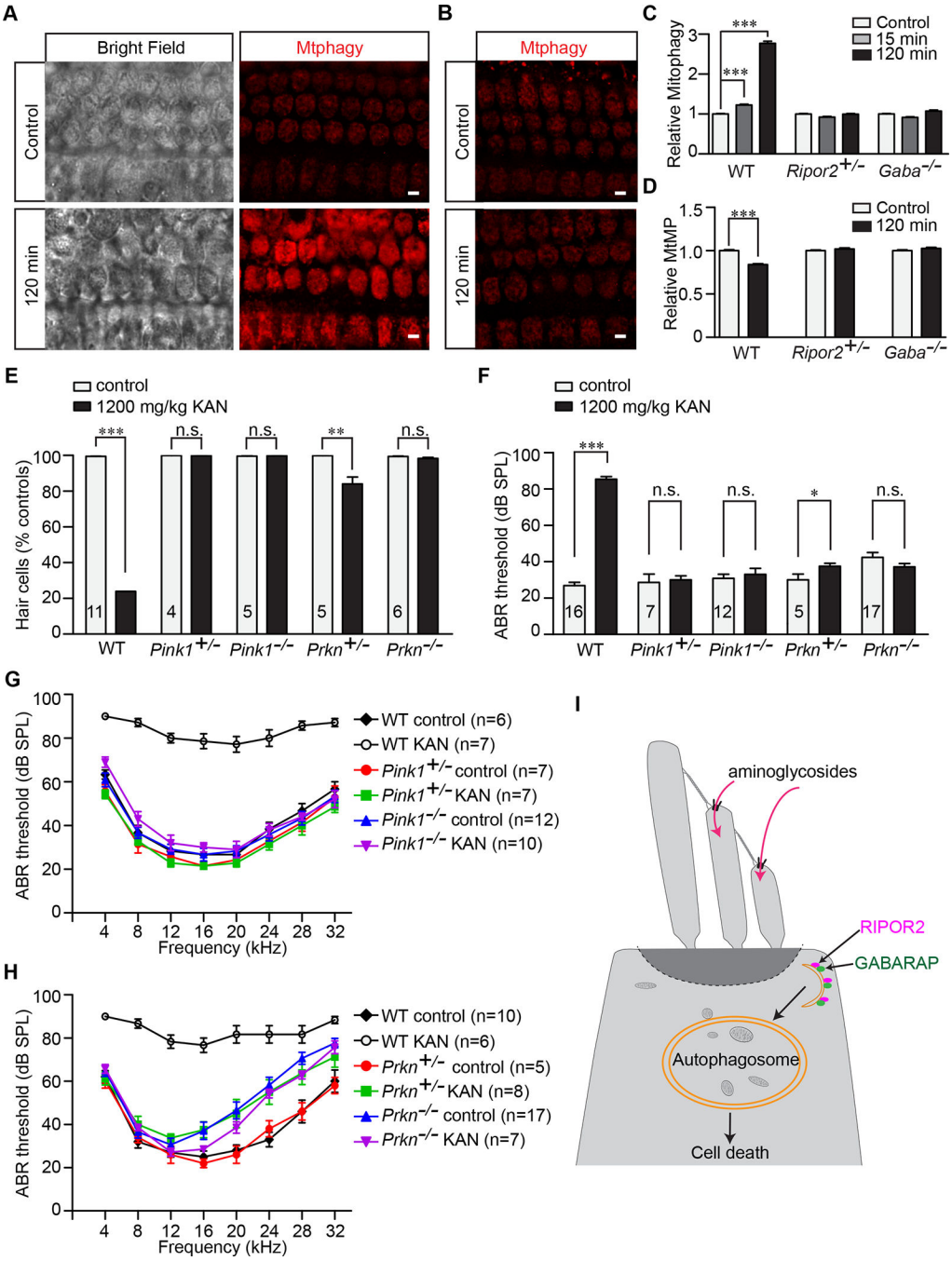

Figure 7. PINK1 and Parkin are required for AG-induced hair cell death and subsequent hearing loss.

(A-B) P4 wild-type (A) or *Ripor2*$^{+/-}$ (B) cochlear explants were treated with 1 mM GEN, and labeled with Mtphagy dye. Scale bars: 5 μm. **(C)** Quantification of Mtphagy dye intensity in wild-type, *Ripor2*$^{+/-}$ and *Gabarap*$^{-/-}$ hair cells. The experiments were repeated at least three times, and in each group more than 300 hair cells from at least three mice were measured. **(D)** P4 wild-type, *Ripor2*$^{+/-}$ or *Gabarap*$^{-/-}$ cochlear explants were treated with 1 mM GEN, and labeled with MT-1, a dye used to monitor mitochondrial membrane

potential (MtMP) in live cells. MtMP was then quantified. The experiments were repeated at least three times, and in each group more than 300 hair cells from at least three mice were measured. **(E)** Percentage of surviving hair cells in wild-type, *Pink1*$^{+/-}$, *Pink1*$^{-/-}$, *Prkn*$^{+/-}$ and *Prkn*$^{-/-}$ mice following KAN treatment. Analyzed mouse numbers are indicated. **(F)** ABR thresholds for click stimuli in wild-type, *Pink1*$^{+/-}$, *Pink1*$^{-/-}$, *Prkn*$^{+/-}$ and *Prkn*$^{-/-}$ mice. Analyzed mouse numbers are indicated. n.s., not significant, *$p < 0.05$, **$p < 0.01$, ***$p < 0.001$ by Student's t test (E, F). **(G)** ABR thresholds for pure tones in wild-type, *Pink1*$^{+/-}$ and *Pink1*$^{-/-}$ mice. Analyzed mouse numbers are indicated. $p < 0.001$ between control and KAN-treated wild-type mice; no significant difference between control and KAN-treated *Pink1*$^{+/-}$ or *Pink1*$^{-/-}$ mice (two-way ANOVA). **(H)** ABR thresholds for pure tones in wild-type, *Prkn*$^{+/-}$ and *Prkn*$^{-/-}$ mice. Analyzed mouse numbers are indicated. $p < 0.001$ between control and KAN-treated wild-type mice; $p < 0.05$ between control and KAN-treated *Prkn*$^{+/-}$ mice; no significant difference between control and KAN-treated *Prkn*$^{-/-}$ mice (two-way ANOVA). **(I)** Model of the functions of RIPOR2 in AG ototoxicity. AG triggers the translocation of RIPOR2, which binds to GABARAP in the pericuticular area, results in the dysfunction of mitophagy and eventually hair cell death.

Key RESOURCES TABLE

REAGENT or RESOURCE	SOURCE	IDENTIFIER
Antibodies		
Anti-RIPOR2	Generated in this study	n/a
Anti-taperin	Sigma	Cat# HPA020899 RRID: AB_1845835
Anti-GRXCR2	Sigma	Cat# HPA059421 RRID: AB_2684010
Anti-CLIC5	Alomone Labs	Cat# ACL-025 RRID: AB_2340921
Anti-GABARAP	Provided by Drs. Regina Feederle and Andrew Flatley at Helmholtz Zentrum Munich, and Dr. Silke Hoffmann at Forschungszentrum Jülich	Cat# GABA 8H5 RRID: AB_2904599
Anti-GABARAP	Abgent	Cat# AP1821a-ev RRID: AB_627695
Anti-GEN	QED Bioscience	Cat# 16102 RRID: AB_129636
Anti-HA	Cell Signaling	Cat# 2367S RRID: AB_10691311
Anti-LC3β	Abcam	Cat# ab51520, RRID: AB_881429
Ant-α-tubulin	Sigma	Cat# T6199, RRID: AB_477583
Anti-Myc	Santa Cruz	Cat# sc-40 RRID: AB_627268
Anti-GFP	Santa Cruz	Cat# sc-9996 RRID: AB_627695
Anti-β2 spectrin	Santa Cruz	Cat# SC-136074 RRID: AB_2194501
Goat anti-Rabbit IgG Secondary Antibody, Alexa Fluor 488	ThermoFisher Sci	Cat# A11070 RRID: AB_2534114
Goat anti-Rat IgG Secondary Antibody, Alexa Fluor 488	ThermoFisher Sci	Cat# A-11006 RRID: AB_2534074
Goat anti-Rabbit IgG Secondary Antibody, Alexa Fluor 546	ThermoFisher Sci	Cat# A11071 RRID: AB_2534115
Goat anti-Rat IgG Secondary Antibody, Alexa Fluor 546	ThermoFisher Sci	Cat# A-11081 RRID: AB_2534125
Amersham ECL Rabbit IgG, HRP-linked whole Ab	GE Healthcare	Cat# NA934 RRID: AB_2722659
Amersham ECL Mouse IgG, HRP-linked whole Ab	GE Healthcare	Cat# NXA931 RRID: AB_772209
Bacterial and Virus Strains		
Subcloning Efficiency™ DH5α™ Competent Cells	ThermoFisher Sci	Cat# 18265017
BL21 (DE3)	ThermoFisher Sci	Cat# EC0114
MAX Efficiency™ Stbl2™ Competent Cells	ThermoFisher Sci	Cat# 10268019
NMY51 Yeast reporter strain	Dualsystem Biotech	Cat# P01004
Chemicals, Peptides, and Recombinant Proteins		
Alexa Fluor™ 488 Phalloidin	ThermoFisher Sci	Cat# A12379
Alexa Fluor™ 568 phalloidin	ThermoFisher Sci	Cat# A12380
Alexa Fluor™ 647 phalloidin	ThermoFisher Sci	Cat# A22287
Thermo Scientific™ Pierce™ ECL 2 Western Blotting Substrate	Fisher Scientific	Cat# PI80196
mitophagy Detection Kit	Dojindo Molecular Tech.	Cat# MD01-10
DAPGreen - Autophagy Detection	Dojindo Molecular Tech.	Cat# D676-10

REAGENT or RESOURCE	SOURCE	IDENTIFIER
MT-1 MitoMP Detection Kit	Dojindo Molecular Tech.	Cat# MT13-10
HisPur™ Ni-NTA Resin	ThermoFisher Sci	Cat# 88222
Strep-Tactin Sepharose	IBA	Cat# 2-1201-010
gentamicin	ThermoFisher Sci	Cat# J62834.06
gentamicin	Sigma	Cat# G1264
kanamycin	ThermoFisher Sci	Cat# J17924.14
kanamycin	Sigma	Cat# K1377
amikacin	ThermoFisher Sci	Cat# J63862.14
neomycin	Fisher Scientific	Cat# 48-012-5GM
streptomycin	ThermoFisher Sci	Cat# 455340050
apramycin	ThermoFisher Sci	Cat# J6661603
cycloheximide	ThermoFisher Sci	Cat# 357420010
H_2O_2	Sigma	Cat# 216763-100ML
GSH	Fisher Scientific	Cat# ICN10181425
D-Methionine	ThermoFisher Sci	Cat# 227210050
Benzamil	Fisher Scientific	Cat# 33-801-0
X-gal	Fisher Scientific	Cat# BP1615-1
32% Paraformaldehyde	Electron Microscopy Sciences	Cat# 15714
25% glutaraldehyde	Electron Microscopy Sciences	Cat# 16220
4% OsO_4 solution	Electron Microscopy Sciences	Cat# 19150
Taq DNA Polymerase w/ Thermo Pol Buffer	New England Biolabs	Cat# M0267X
Deoxynucleotide Solution	New England Biolabs	Cat# N0446S
Platinum Pfx DNA Polymerase	ThermoFisher Sci	Cat# 11708013
HBSS	ThermoFisher Sci	Cat# 14175103
DMEM	ThermoFisher Sci	Cat# 11965118
DMEM/F-12	ThermoFisher Sci	Cat# 11039047
Fetal bovine serum	Fisher Scientific	Cat# MT35010CV
Penicillin Streptomycin Solution	Fisher Scientific	Cat# MT30002CI
EZview™ Red Anti-HA Affinity Gel	Sigma	Cat#E6779
Experimental Models: Cell Lines		
HEK293	ATCC	Cat# CRL-1573
HEI-OC1	Provided by Dr. Federico Kalinec at University of California, Los Angeles	RRID: CVCL_D899
Experimental Models: Organisms/Strains		
Mouse: C57BL/6J	The Jackson Laboratory	Cat# 000664
Mouse: *Ripor2*$^{-/-}$	Zhao et al., 2016	MGI:5085529
Mouse: *Tmie*$^{-/-}$	Zhao et al., 2014	MGI:5784557
Mouse: *Grxcr2*$^{-/-}$	Liu et al., 2018	MGI:6281113
Mouse: *Gabarap*$^{-/-}$	MMRRC	MGI:3530477

REAGENT or RESOURCE	SOURCE	IDENTIFIER
Mouse: *LC3β*$^{-/-}$	The Jackson Laboratory	MGI:3774111
Mouse: *Pink1*$^{-/-}$	The Jackson Laboratory	MGI:3716083
Mouse: *Prkn*$^{-/-}$	The Jackson Laboratory	MGI:2681404
Oligonucleotides		
Genotyping primers for *Ripor2*$^{-/-}$ mice: 5'- TTAGGCTTAGGAGCCCTGTG -3', 5'-TATCAGCTCTCCAGAGGCAGTC -3', 5'-GGTAAACTGGCTCGGATTAGGG -3' and 5'-TTGACTGTAGCGGCTGATGTTG -3'	Integrated DNA Technologies	n/a
Genotyping primers for *Tmie*$^{-/-}$ mice: 5'-GGCTCGGTATCTACAGCGAAAGGCGGCC -3' and 5'-TGCCTGGCTCTGACTAGTTTCTGCAC -3'	Integrated DNA Technologies	n/a
Genotyping primers for *Grxcr2*$^{-/-}$ mice: 5'- TCTTCCTACAGTGGCCGAGT -3' and 5'-TGAATGTGAGCGAGATACCG -3'	Integrated DNA Technologies	n/a
Genotyping primers for *Gabarap*$^{-/-}$ mice: 5'- ACTTGATACTGCTGCCTCGG -3', 5'-CCTCATCCTGAATGGTGACA -3' and 5'-CCTTGCAAAATGGCGTTACT -3'	Integrated DNA Technologies	n/a
Genotyping primers for *LC3β*$^{-/-}$ mice: 5'- GACACCTGTACACTCTGATGCACT -3', 5'-CCTGCCGTCTGCTCTAAGCTG -3' and 5'-CCACTCCCACTGTCCTTTCCTAAT -3'	Integrated DNA Technologies	n/a
Genotyping primers for *Pink1*$^{-/-}$ mice: 5'- TCGAGGGACCTAATAACTTCG -3', 5'-GCGGCGACTCTGCTCTATAC -3' and 5'-GCCATATCCACTGCAGGTCT -3'	Integrated DNA Technologies	n/a
Genotyping primers for *Prkn*$^{-/-}$ mice: 5'- CCTACACAGAACTGTGACCTGG -3', 5'-GCAGAATTACAGCAGTTACCTGG -3' and 5'-ATGTTGCCGTCCTCCTTGAAGTCG -3'	Integrated DNA Technologies	n/a
Cloning primers for GABARAP: 5'-GCTAGTCGACATGAAGTTCGTGTACAAAGAG -3' and 5'-GTGCGGCCGCTCACAGACCATAGACGCTTTC -3'	Integrated DNA Technologies	n/a
Cloning primers for GABARAPL1: 5'-GCTAGTCGACATGAAGTTCCAGTATAAGGAG -3' and 5'-GTGCGGCCGCTCATTTTCCATAGACACTTTC -3'	Integrated DNA Technologies	n/a
Cloning primers for LC3β: 5'-GCTAGGATCCATGCCGTCCGAGAAGACCTT -3' and 5'-GTGCGGCCGCTTACACAGCCATTGCTGTCC -3'	Integrated DNA Technologies	n/a
Recombinant DNA		
HA-RIPOR2	Zhao *et al.*, 2016	n/a
RIPOR2-GFP	Zhao *et al.*, 2016	n/a
HA-GABARAP	This study	n/a
HA-GABARAPL1	This study	n/a
HA-LC3β	This study	n/a
Myc-GRXCR2	Liu *et al.*, 2018	n/a
Myc-taperin	Zhao *et al.*, 2016	n/a
CLIC5-GFP	Li *et al.*, 2021	n/a
Software and Algorithms		
Prism 7	Graphpad	https://www.graphpad.com/

REAGENT or RESOURCE	SOURCE	IDENTIFIER
Vector NTI	Invitrogen	https://www.thermofisher.com/us/en/home/life-science/cloning/vector-nti-software.html
ImageJ	NIH	https://imagej.nih.gov/ij/